

## Supporting Information

# Facile and selective polynitrations at the 4-pyrazolyl dual backbone: A straightforward access to a series of high-density energetic materials

*Kostiantyn V. Domasevitch,<sup>a\*</sup> Ivan Gospodinov,<sup>b</sup> Harald Krautscheid,<sup>c</sup> Thomas M. Klapötke,<sup>b\*</sup> Jörg Stierstorfer<sup>b</sup>*

<sup>a</sup> Inorganic Chemistry Department, Taras Shevchenko National University of Kyiv, Volodymyrska Str. 64/13, Kyiv 01601, Ukraine

<sup>b</sup> Ludwig-Maximilian University Munich, Department of Chemistry, Butenandtstr. 5-13 (D), 81377 München, Germany. Homepage: <http://www.hedm.cup.uni-muenchen.de>

<sup>c</sup> Institut für Anorganische Chemie, Universität Leipzig, Johannisallee 29, D-04103 Leipzig, Germany

## Table of Contents

1. Experimental Procedures .....	2
2. X-ray Diffraction .....	3
Crystal Data Table	
Detailed description of crystal structures	
3. Computations .....	20
4. Small-scale shock reactivity test (SSRT) .....	21
5. Thermal stability .....	22
6. NMR spectroscopy .....	27
7. References .....	33

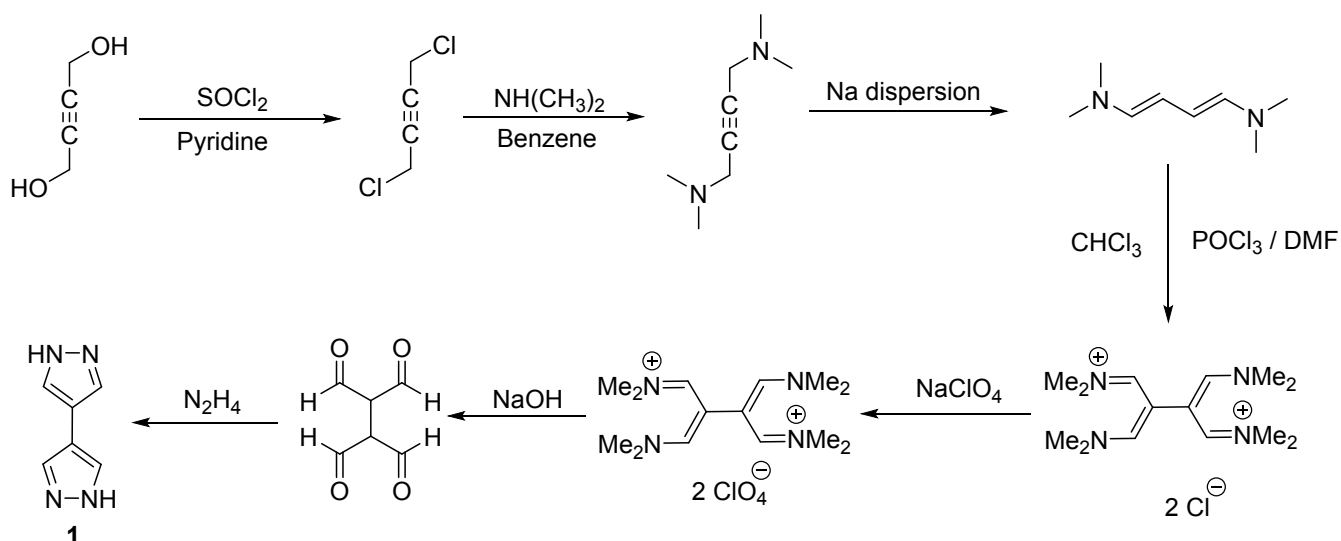
# 1. Experimental Procedures

## 1.1. General Procedures

$^1\text{H}$  and  $^{13}\text{C}$  NMR spectra were recorded on *JEOL 270* and *BRUKER AMX 400* instruments. The samples were measured at room temperature in standard NMR tubes ( $\text{\O} 5 \text{ mm}$ ). Chemical shifts are reported as  $\delta$  values in ppm relative to the residual solvent peaks *d*<sub>6</sub>-DMSO ( $\delta_{\text{H}}$ : 2.50,  $\delta_{\text{C}}$ : 39.5). Solvent residual signals and chemical shifts for NMR solvents were referenced against tetramethylsilane (TMS,  $\delta = 0 \text{ ppm}$ ) and nitromethane. Unless stated otherwise, coupling constants were reported in hertz (Hz) and for the characterization of the observed signal multiplicities the following abbreviations were used: s (singlet), d (doublet), t (triplet), q (quartet), quint (quintet), sept (septet), m (multiplet) and br (broad). Low resolution mass spectra were recorded on a *JEOL JMS-700 MStation* mass spectrometer (EI+/DEI+). Infrared spectra (IR) were recorded from  $4500 \text{ cm}^{-1}$  to  $650 \text{ cm}^{-1}$  on a PERKIN ELMER Spectrum BX-59343 instrument with *SMITHS DETECTION DuraSamplIR II Diamond ATR* sensor. The absorption bands are reported in wavenumbers ( $\text{cm}^{-1}$ ). Elemental analysis was carried out by the department's internal micro analytical laboratory on an *Elementar Vario el* by pyrolysis of the sample and subsequent analysis of the formed gases. All sensitivities toward impact (IS) and friction (FS) were determined according to BAM (German: Bundesanstalt für Materialforschung und Prüfung) standards using a BAM drop hammer and a BAM friction apparatus.<sup>[S1]</sup> Compounds **2–6** and **6**·H<sub>2</sub>O were tested for sensitivity towards electrical discharge using an Electric Spark Tester ESD 2010 EN.

## 1.2. Synthesis

The synthesis of **1** was performed by the literature known method<sup>[S2]</sup> starting with readily available and inexpensive industrial product 2-butyne-1,4-diole. This simple (and easily scalable for bulk preparations) procedure was essentially a compilation of literature methods for preparation of 1,4-dichloro-2-butyne, either with  $\text{SOCl}_2$ <sup>[S3]</sup> or  $\text{POCl}_3$ <sup>[S4]</sup> as the reagents; preparation of 1,4-*bis*(dimethylamino)butyne<sup>[S5,6]</sup> and its rearrangement into the conjugated *cis-trans*-butadiene over Na metal dispersion<sup>[S6]</sup> and the subsequent Vilsmeier-Haack-Arnold formylation providing symmetric *bis*-trimethinium salt (isolated and purified as perchlorate salt).<sup>[S7]</sup> The latter was hydrolyzed to *bis*-dialdehyde and then converted into the desired 4,4'-bipyrazole (**1**).



**Scheme S1.** Performed synthesis for 4,4'-bipyrazole (**1**) according to the known literature.

## 2. X-ray Diffraction

The diffraction data were collected with graphite-monochromated Mo K $\alpha$  radiation ( $\lambda = 0.71073 \text{ \AA}$ ) using a Stoe Image Plate Diffraction System,  $\varphi$  oscillation scans (typically,  $\varphi 0 \rightarrow 180^\circ$ ;  $\Delta\varphi = 0.8\text{-}0.9^\circ$ ; exposure times 7-8 min per frame).<sup>[S8]</sup> For **1** and **5**, the data were collected with IPDS-2T diffractometer. The structures were solved by direct methods and refined by full-matrix least-squares on  $F^2$  using the programs SHELXS-97 and SHELXL-2014/7.<sup>[S9]</sup> All the CH-hydrogen atoms were located and freely refined with isotropic thermal parameters. Table S1 lists main crystallographic data and parameters of crystal structure refinement. Graphical visualization of the structure was made using the program Diamond 2.1e,<sup>[S10]</sup> and the topological analysis was performed using TOPOS 4.0.<sup>[S11]</sup>

The most important molecular geometry parameter, which is sensitive to the progressive nitro substitution at the 4,4'-bipyrazole platform, is dihedral angle (twist angle)  $\varphi$  subtended by mean planes of two pyrazole halves. Unsubstituted 4,4'-bipyrazole is exactly planar, while lying across a center of inversion in the crystal,<sup>[S2]</sup> and the molecule of mononitro derivative **2** retains appreciably flat structure [ $\varphi = 5.63(12)^\circ$ ] as well. With the second nitro group, either in the case of 3,5- or 3,3'-derivatives, the bipyrazole core loses planarity [ $\varphi = 46.48(4)$  and  $50.28(5)^\circ$ , for **2** and **3**, respectively], but similar effect from further substitution (**2**, **3**  $\rightarrow$  **4**  $\rightarrow$  **5**) is much weaker (Table S2). Moreover, the mutual orientation of two pyrazole rings for **4** and **5** does not differ significantly [ $\varphi = 50.28(5)$  vs.  $58.58(9)^\circ$ ] and thus the third and fourth NO<sub>2</sub> groups installed at the molecular frame do not lead to essential steric strains. This situation may be compared with conformations of 4,4'-bipyrazole and its 3,3'-dimethyl- [ $\varphi = 5\text{-}30^\circ$ ]

**Table S1.** Crystal data for compounds **2-6** and **6·H<sub>2</sub>O**.

	<b>2</b>	<b>3</b>	<b>4</b>	<b>5</b>	<b>6</b>	<b>6·H<sub>2</sub>O</b>
Formula	C <sub>6</sub> H <sub>5</sub> N <sub>5</sub> O <sub>2</sub>	C <sub>6</sub> H <sub>4</sub> N <sub>6</sub> O <sub>4</sub>	C <sub>6</sub> H <sub>4</sub> N <sub>6</sub> O <sub>4</sub>	C <sub>6</sub> H <sub>3</sub> N <sub>7</sub> O <sub>6</sub>	C <sub>6</sub> H <sub>2</sub> N <sub>8</sub> O <sub>8</sub>	C <sub>6</sub> H <sub>4</sub> N <sub>8</sub> O <sub>9</sub>
<i>M</i>	179.15	224.15	224.15	269.15	314.16	332.17
<i>T</i> /K	173	213	213	213	203	213
Color and habit	Orange plate	Pale-yellow prism	Pale-yellow plate	Colorless prism	Colorless prism	Colorless block
Size / mm	0.26 × 0.24 × 0.22	0.26 × 0.24 × 0.20	0.27 × 0.25 × 0.22	0.22 × 0.18 × 0.17	0.28 × 0.22 × 0.20	0.27 × 0.24 × 0.23
Crystal system	Tetragonal	Monoclinic	Monoclinic	Monoclinic	Tetragonal	Monoclinic
Space group	<i>P</i> 4 <sub>1</sub> 2 <sub>1</sub> 2 (No. 92)	<i>C</i> 2/ <i>c</i> (No. 15)	<i>C</i> 2/ <i>c</i> (No. 15)	<i>P</i> 2 <sub>1</sub> / <i>c</i> (No. 14)	<i>P</i> 4 <sub>2</sub> / <i>n</i> (No. 86)	<i>C</i> <i>c</i> (No. 9)
<i>Z</i>	8	4	4	4	8	4
<i>a</i> / Å	5.4831(2)	15.9744(9)	6.1653(7)	8.6064(8)	16.4281(13)	11.1017(9)
<i>b</i> / Å	5.4831(2)	6.5428(8)	15.7789(12)	11.9636(9)	16.4281(13)	13.9227(10)
<i>c</i> / Å	47.463(3)	8.9414(8)	8.7387(10)	10.1200(9)	8.3705(6)	8.2166(8)
$\alpha$ / °	90	90	90	90	90	90
$\beta$ / °	90	118.739(10)	107.434(10)	114.148(10)	90	110.654(10)
$\gamma$ / °	90	90	90	90	90	90
<i>V</i> / Å <sup>3</sup>	1426.95(12)	819.41(13)	811.06(14)	950.81(14)	2259.1(3)	1188.38(17)
$\mu$ (Mo-K $\alpha$ )/ mm <sup>-1</sup>	0.132	0.156	0.157	0.170	0.172	0.175
<i>D</i> <sub>calc</sub> / g cm <sup>-3</sup>	1.668	1.817	1.836	1.880	1.847	1.857
2 $\theta$ <sub>max</sub> / °	27.95	28.03	27.94	28.01	28.28	27.99
Measd/ Unique reflns	6517 / 1701	3236 / 986	3458 / 959	8130 / 2294	9974 / 2783	5099 / 2319
Completeness/ %	98.8	99.0	98.5	997	992	982
Reflns with <i>I</i> > 2 $\sigma$ ( <i>I</i> )	1584	829	835	1365	2122	2059
<i>R</i> <sub>int</sub>	0.035	0.023	0.024	0.043	0.041	0.017
Parameters refined	138	81	82	184	207	224
<i>R</i> 1, <i>wR</i> 2 ( <i>I</i> > 2 $\sigma$ ( <i>I</i> ))	0.032, 0.078	0.037, 0.094	0.034, 0.090	0.038, 0.081	0.034, 0.080	0.021, 0.049
<i>R</i> 1, <i>wR</i> 2 (all data)	0.034, 0.079	0.042, 0.097	0.039, 0.091	0.070, 0.086	0.049, 0.083	0.024, 0.050
Goof on <i>F</i> <sup>2</sup>	1.102	1.045	1.089	0.814	1.001	0.936
Max, min peak/ e Å <sup>-3</sup>	0.16, -0.13	0.29, -0.24	0.34, -0.19	0.22, -0.20	0.23, -0.24	0.15, -0.11
CCDC	1836403	1836404	1836405	1836406	1836407	1836408

and 3,3',5,5'-tetramethyl [ $\varphi = 60-90^\circ$ ] derivatives in many examined salts<sup>[S12]</sup> and coordination compounds.<sup>[S13]</sup>

Unlike these very individual conformational features, the bond lengths and bond angles are less sensitive to the progressive nitro substitution and the corresponding parameters for 4,4'-bipyrazole,<sup>[S2]</sup> **2-6** and **6** · H<sub>2</sub>O appear to be actually uniform. In particular, the central C-C bond lengths are nearly identical for all the species, when lying within the narrow range of 1.4589(19)-1.467(2) Å (Table S2). These bonds are very similar even in the case of **3** and **4** (existing as pyrazolium/pyrazolate zwitterion) [1.4589(19) and 1.4621(19) Å, respectively]. Very subtle differences in the bond lengths parameters may be detected for the pyrazole N-N bonds, which experience certain shortening as the number of nitro group increased [1.32-1.33 Å for dinitropyrazole rings and 1.34-1.35 Å for unsubstituted pyrazole rings, see Table S2].

**Table S2.** Selected geometry parameters for 4,4'-bipyrazole **1**,<sup>[S2]</sup> **2-6** and **6**·H<sub>2</sub>O.

	NO <sub>2</sub> groups	Twist angle/ <sup>o</sup>	d(C-C)/ Å	d(N-N)/ Å for the rings:		
				pyrazole	nitropyrazole	dinitropyrazole
<b>1</b>	0	0	1.464(2)	1.3462(15) × 2	-	-
<b>2</b>	1	5.63(12)	1.462(2)	1.350(2)	1.333(2)	-
<b>3</b>	2	46.48(4)	1.4589(19)	-	1.3334(15) × 2	-
<b>4</b>	2	50.28(5)	1.4621(19)	1.341(2)	-	1.3352(17)
<b>5</b>	3	58.58(9)	1.468(2)	-	1.339(2)	1.323(2)
<b>6</b>	4	71.44(5)	1.4644(15)	-	-	1.3263(16); 1.3321(16)
<b>6</b> ·H <sub>2</sub> O	4	78.99(6)	1.467(2)	-	-	1.320(2); 1.322(2)

## 2.1. Crystal structure of 3-nitro-4,4'-bipyrazole (**2**)

The compound crystallizes in a chiral group *P4*<sub>1</sub>*2*<sub>1</sub>*2* (enantiomorphous to *P4*<sub>3</sub>*2*<sub>1</sub>*2*) (with relatively long period *c* of the unit cell of 47.463(3) Å) and it adopts complicated 3D supramolecular structure, dominated by conventional hydrogen bonding of pyrazole NH donors. These interactions reveal some kind of segregation: two sites of the molecules establish two distinct supramolecular patterns incorporating either pyrazole or nitropyrazole groups only.

The latter motif involves multiple set of bifurcate and weaker interactions (Fig. S1). The N3H group adopts H-bond to nitropyrazole moiety: it utilizes pyrazole N4<sup>ii</sup> and nitro O1<sup>ii</sup> [symmetry code

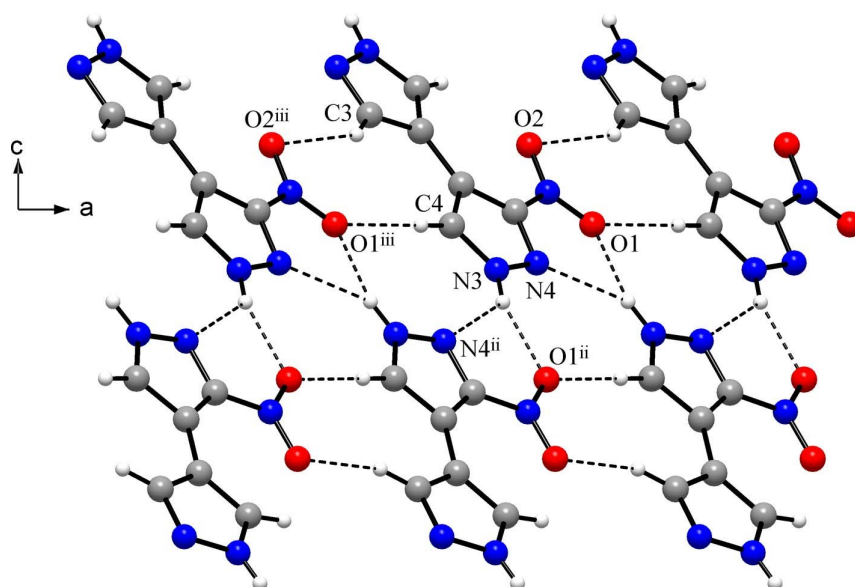


**Figure S1.** Hydrogen bonded motif of the structure of **2** involving nitropyrazole sides of the molecules. Note the bifurcation of the NH...N,O bonds and double CH...O bonding to nitro acceptor [Symmetry codes: (ii)  $y, -1+x, -z$ ; (iii)  $-1+x, -1+y, z$ ].

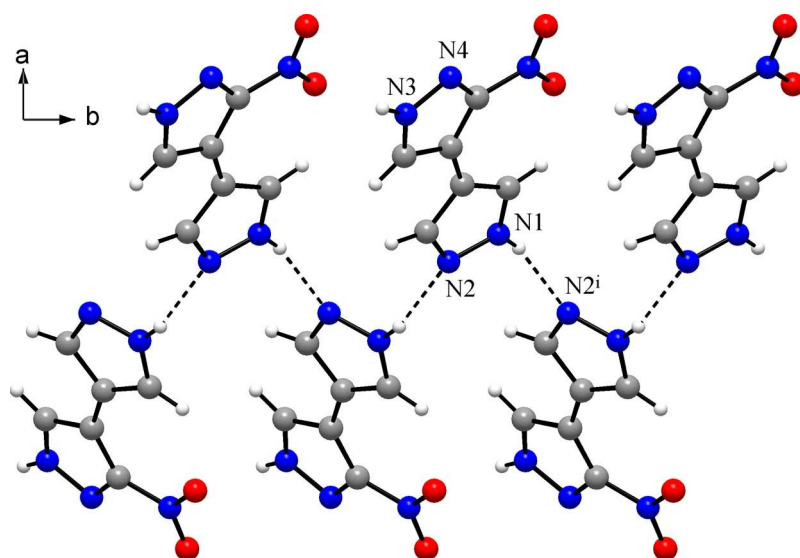


**Figure S2.** Hydrogen bonded motif of the structure of **2** involving pyrazole sides of the molecules, in the form of catemer [Symmetry code: (i)  $-1.5-x, 0.5+y, 0.25-z$ ].

(ii)  $y, -1+x, -z$ ] atoms as acceptors and the N3H...O1<sup>ii</sup> branch of this bifurcate bond is slightly stronger and more directional (Table S3). Weaker CH...O bonds are found between the adjacent pyrazole cycles and nitro group [symmetry code (iii)  $-1+x, -1+y, z$ ]. These interactions connect the molecular into strips, which pack one on the top of another and are interconnected by H-bonds through unsubstituted pyrazole sites of the molecules. This pyrazole connectivity is sustained with relatively short and directional N1H...N2<sup>i</sup> bonds [N...N = 2.8665(17) Å; ∠NH...N = 152.1(11)°; symmetry code (i)  $-1.5-x, 0.5+y, 0.25-z$ ] and it exists in the form of catemer (Fig. S2), very similar to the structure of 4,4'-bipyrazole itself.<sup>[S2]</sup>

The entire H-bonded structure represents 3D framework of exceptional topology. When considering only the strongest interactions of conventional NH donors, every molecule is bonded with four closest neighbors, and thus the uninodal four-coordinated 3D framework with a point (Schläfli) symbol  $\{6^3.8^3\}$  is found [extended point symbol: 6.6.6.8(8).8(4).8(4)] (See Fig. S3). Alternatively, with a single pyrazole cycle as three-connected net node, two NH-hydrogen bonds and central covalent C-C bonds as the net links, the topology may be regarded as binodal 3,3-coordinated net with a point (Schläfli) symbol  $\{10^2.12\}\{10^3\}$ .

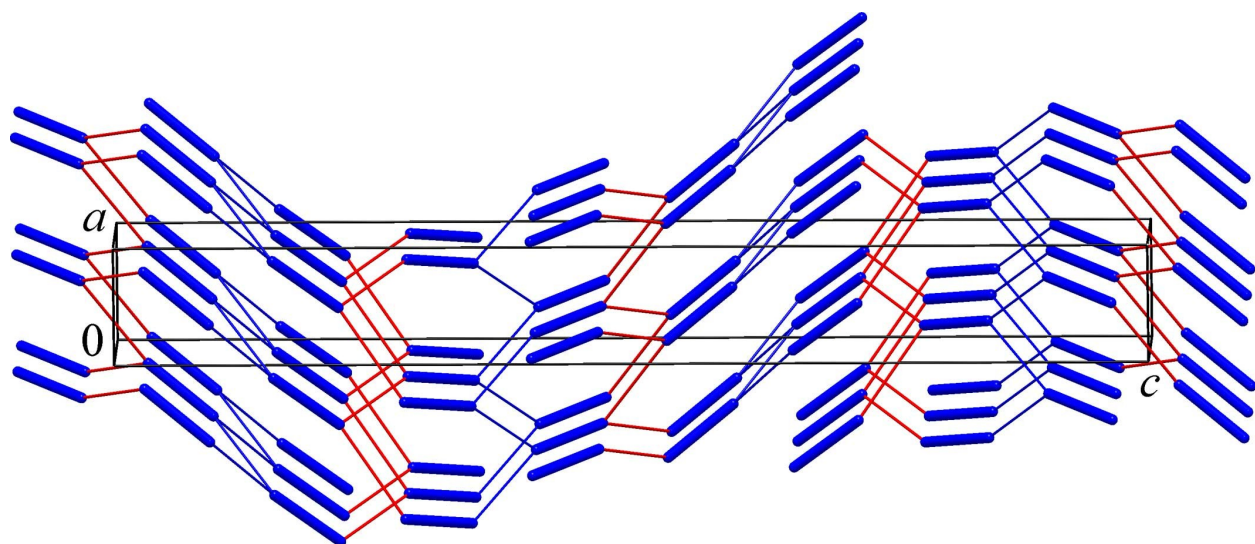


**Figure S3.** Supramolecular connectivity in the structure of **2**: Blue sticks represent molecules of the bipyrazole, thin blue lines are NH...N links of unsubstituted pyrazole sides whereas thin red lines are NH...N,O bonds of nitropyrazole sides. Note very long period of translation along *c* axis [47.463(3) Å].

**Table S3.** Hydrogen-bond geometry (Å, °) for the structure of 3-nitro-4,4'-bipyrazole (**2**).

Donor (D)	Hydrogen (H)	Acceptor (A) <sup>a)</sup>	D-H	H...A	D...A	∠DH...A
N1	H1N	N2 <sup>i</sup>	0.87(2)	2.07(2)	2.8665(17)	152.1(11)
N3	H2N	N4 <sup>ii</sup>	0.89(2)	2.463(19)	3.1272(16)	131.8(15)
N3	H2N	O1 <sup>ii</sup>	0.89(2)	2.04(2)	2.8808(16)	157.6(16)
C1	H1	O2	0.92(2)	2.314(18)	2.8784(18)	119.3(13)
C3	H3	O1 <sup>iii</sup>	0.95(2)	2.76(2)	3.6786(18)	162.1(15)
C3	H3	O2 <sup>iii</sup>	0.95(2)	2.53(2)	3.3657(18)	146.7(15)
C4	H4	O1 <sup>iii</sup>	0.933(19)	2.42(2)	3.3478(17)	175.7(16)

<sup>a)</sup> Symmetry codes: (i) -1.5-x, 0.5+y, 0.25-z; (ii) y, -1+x, -z; (iii) -1+x, -1+y, z.

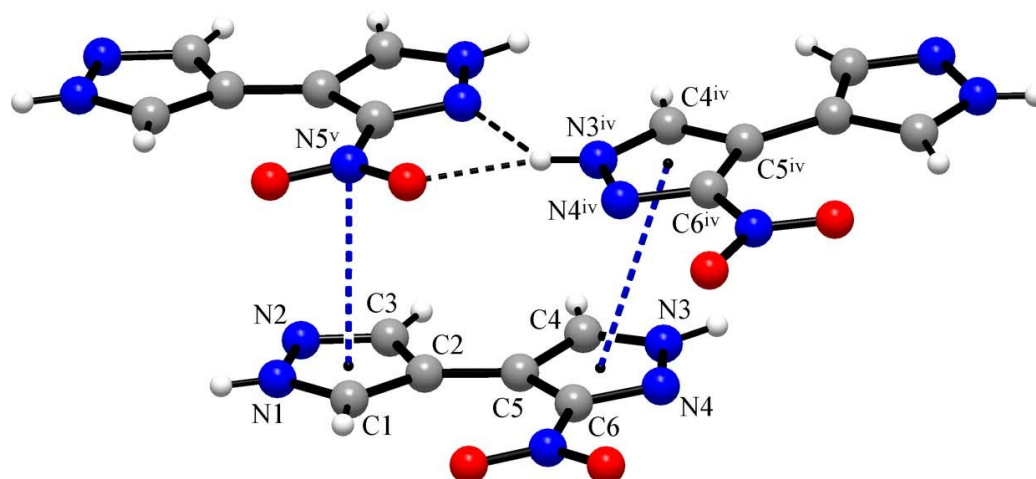


**Figure S4.** Weak stacking interactions in the structure of **2**: slipped  $\pi/\pi$  interaction of two nitropyrazole groups and  $\pi$ -hole/ $\pi$  contact involving nitro group [Symmetry codes: (iv)  $y, x, -z$ ; (v)  $-1+x, y, z$ ].

Structure of **2** is the only example for stacking interactions, within a full set of the examined nitro-4,4'-bipyrazoles. Very weak slipped  $\pi/\pi$  interactions is observed between the nitropyrazole rings (Fig. S4) whereas nitro group establishes contact with the pyrazole ring. The latter one may be attributed to a very weak  $\pi$ -hole/ $\pi$  interaction, with the nitro-N atom situated almost exactly above the ring centroid [ $N\cdots\pi = 3.226(2)$  Å; slippage angle is  $5.07^\circ$ ]. It is not surprising that such kind of interactions occurs for unsubstituted pyrazole ring, but it is totally eliminated for more electron deficient nitropyrazoles (**3-6**).

**Table S4.** Geometry parameters of stacking interactions in the structure of **2**.<sup>a)</sup>

Type	Group 1	Group 2	Shortest contact/ Å	IPD/ Å	CCD/ Å	SA/ °
$\pi/\pi$	(C4C5C6N3N4)	(C4C5C6N3N4) <sup>iv</sup>	3.254(2)	3.265(2)	3.562(2)	23.58
$\text{NO}_2/\pi$	(C1C2C3N1N2)	(N5O1O2) <sup>v</sup>	3.322(2)	3.213(2)	3.226(2)	5.07

<sup>a)</sup> See Fig. S4. IPD is the interplanar distance (distance from one plane to the neighboring centroid), CCD is the centre-to-centre distance (distance between ring centroids), SA is the slippage angle (angle subtended by the intercentroid vector to the plane normal). For  $\text{NO}_2/\pi$  stacking, IPD and CCD refer to distances between plane of Group 1 and  $\text{N5}^v$ ; and distance between centroid of Group 1 and  $\text{N5}^v$ , respectively [Symmetry codes: (iv)  $y, x, -z$ ; (v)  $-1+x, y, z$ .]

## 2.2. Crystal structure of 3,3'-dinitro-4,4'-bipyrazole (3)

The compound crystallizes in space group  $C2/c$  and the molecule resides on a two-fold axis passing through the centroid of the central C-C bond. Thus two pyrazole halves of the molecules are symmetry equivalent. This causes significant simplification of the supramolecular array, as may be compared with the previous structure. Loss of the coplanarity of two pyrazole rings, now subtending dihedral angle of  $46.48(4)^\circ$ , is also an important factor. First, this eliminates stacking interactions, which are favorable for packing of flat molecules. Second, the twisted structure mitigates against efficiency of double  $\text{CH}\cdots\text{O}$  bonding from two pyrazole rings to a nitro acceptor seen in the structure of **2**. The primary supramolecular pattern in **3** exists as 2D flat four-connected network parallel to a  $ab$  plane, which is sustained with a set of bifurcate  $\text{NH}\cdots\text{N},\text{O}$  bonds (Fig. S5). Two branches of such bonds are nearly identical in the view of  $\text{D}\cdots\text{A}$  separations [ $\text{N}\cdots\text{N} = 3.0433(13)$  vs.  $\text{N}\cdots\text{O} = 2.9946(13)$  Å], although interaction with N-acceptor is more directional [ $\angle\text{NH}\cdots\text{N} = 160.9(16)^\circ$  vs.  $\angle\text{NH}\cdots\text{O} = 128.4(15)^\circ$ , Table S5]. This is accompanied with a set of very weak  $\text{CH}\cdots\text{O}$  bonds [ $\text{C}\cdots\text{O} = 3.5742(17)$  and  $3.6982(16)$  Å], which are also bifurcated and one of these branches is involved for connection of successive layers, separated at  $3.92$  Å (Fig. S6). It worths noting that within the single layer the orientation of the molecules is identical and therefore the layer is polar. However, polarities of separate layers compensate each other by anti-alignment.

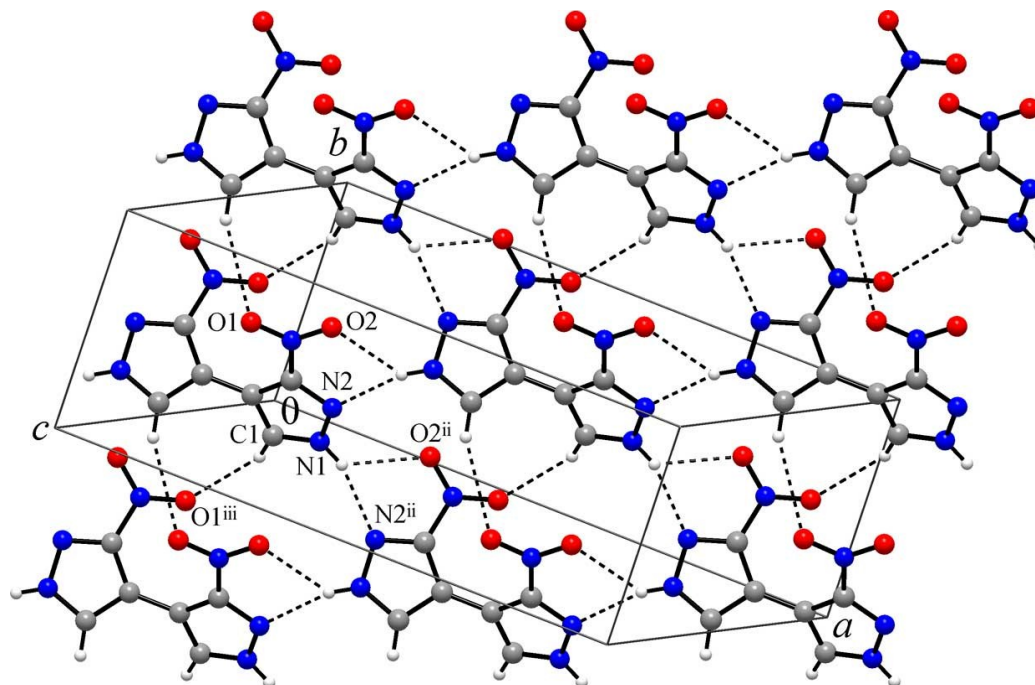


**Figure S5.** Fragment of the structure of **3** showing the flat hydrogen bonded network, which is parallel to a  $ab$  plane. [Symmetry codes: (ii)  $0.5-x, -0.5+y, 0.5-z$ ; (iii)  $-x, -1+y, 0.5-z$ ].

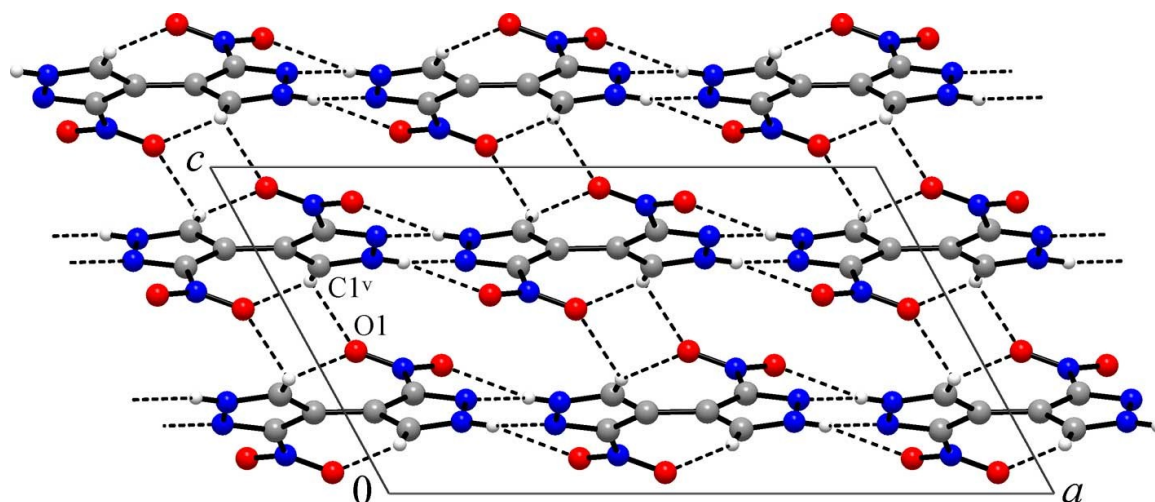


**Figure S6.** Projection on a *ac* plane: Packing of successive layers in the structure of **3**, with a set of very weak interlayer CH...O bonding [Symmetry code (v)  $x, -y, 0.5+z$ ].

**Table S5.** Hydrogen-bond geometry ( $\text{\AA}$ ,  $^\circ$ ) for structure of 3,3'-dinitro-4,4'-bipyrazole **3**.

Donor (D)	Hydrogen (H)	Acceptor (A) <sup>a)</sup>	D-H	H...A	D...A	$\angle\text{DH}\cdots\text{A}$
N1	H1N	N2 <sup>ii</sup>	0.869(18)	2.208(18)	3.0433(13)	160.9(16)
N1	H1N	O2 <sup>ii</sup>	0.869(18)	2.376(18)	2.9946(13)	128.4(15)
C1	H1	O1 <sup>iii</sup>	0.951(16)	2.803(16)	3.6982(16)	157.2(11)
C1	H1	O1 <sup>iv</sup>	0.951(16)	2.794(16)	3.5742(17)	139.9(11)

<sup>a)</sup> Symmetry codes: (ii)  $0.5-x, -0.5+y, 0.5-z$ ; (iii)  $-x, -1+y, 0.5-z$ ; (iv)  $x, -y, -0.5+z$ .

### 2.3. Crystal structure of 3,5-dinitro-4,4'-bipyrazole (**4**)

3,5-Dinitrocompound presents a particular example, since basic pyrazole site and appreciably acidic 3,5-dinitropyrazole ( $\text{p}K_a = 3.14$  for 3,5-dinitropyrazole<sup>[S14]</sup>) site appear incompatible within the molecule and the latter exists rather in a peculiar pyrazolium/dinitropyrazolate zwitter-ionic form. The compound crystallizes in  $C2/c$  space group and the molecule lies on a 2-fold axis passing through the central C-C bond and centroids of pyrazolium and dinitropyrazolate N-N bonds. That the symmetry equivalence of two nitrogen sites for every of the rings is not an apparent effect of equal disorder of two protons, may be illustrated by the results of mean-square displacement amplitude analysis, which provides a sensitive parameter for unambiguous detection of subtle effects of the disorder.<sup>[S15]</sup> Absolute differences of ADPs along the directions of the bonds are calculated using *THMA11*<sup>[S16]</sup> and they essentially fit a limit of  $0.0010 \text{ \AA}^2$  suggested by Hirshfeld for rigid bonds (in particular, for N1-C1 and N2-C4  $|\Delta\text{ADP}|$  are  $0.0012(7)$  and  $0.0002(7) \text{ \AA}^2$ , respectively).

The zwitter-ionic pyrazolium/dinitropyrazolate structure of the molecule has clear impact for the hydrogen bonding: instead of a set of weaker H-bond donors and acceptors in the structure of **3**, one can find now a combination of very potent functionalities in the form of highly acidic polarized pyrazolium-NH<sup>+</sup> and anionic pyrazolate-N<sup>-</sup> sites. Such difference is essential for more strong hydrogen bonding in the structure of **4**. First, bifurcation of the bonding between N and O acceptors disappears and actually only strong and directional bond to a more competitive N-site is established [ $\angle\text{NH}\cdots\text{N} = 165.4(19)^\circ$  vs.  $\angle\text{NH}\cdots\text{O} = 120.2(16)^\circ$ , Table S6]. Second, this NH $\cdots$ N bond is significantly stronger than the one in the structure of **3** (N $\cdots$ N separations are 2.8410(14) and 3.0433(13) Å, respectively). Therefore, in spite of a somewhat greater molecular twist angle, packing of 3,5-isomer (**4**) is even slightly more dense than the packing of 3,3'-isomer (**3**), as is suggested by crystal densities (1.836 and 1.817 g cm<sup>-3</sup>) and packing indices (76.6 and 76.5, respectively).

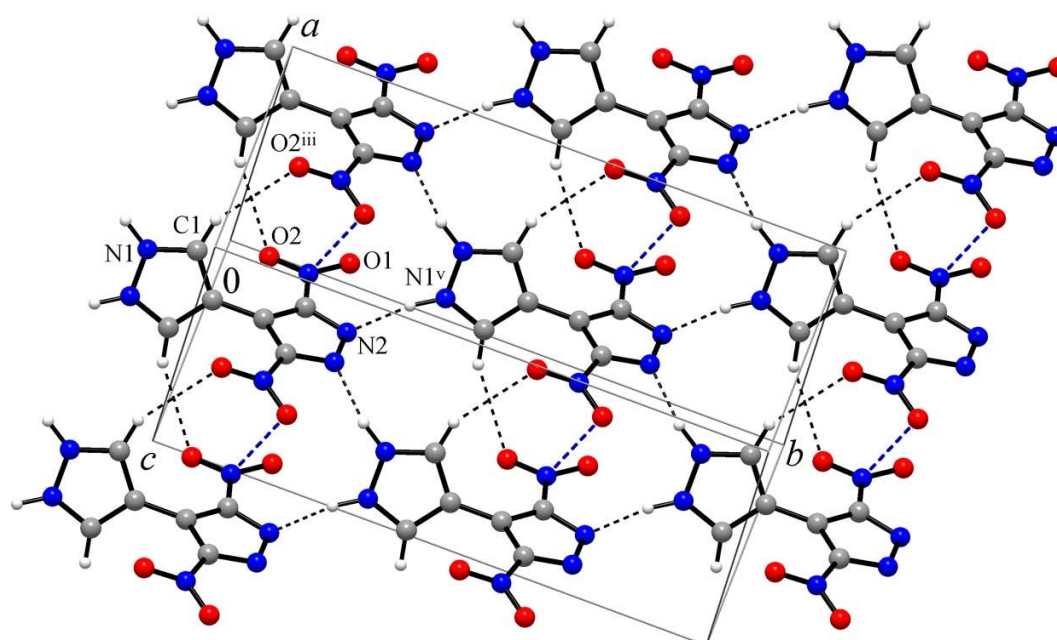


**Figure S7.** Fragment of hydrogen bonded layer in the structure of **4**, with dotted lines indicating H-bonds and intermolecular  $\pi$ -hole/lone pair interactions. [Symmetry codes: (iii)  $1-x, y, 0.5-z$ ; (v)  $0.5-x, 0.5+y, 0.5-z$ ].

Second important consequence of the zwitter-ionic pyrazolium/dinitropyrazolate structure of **4** is strict mutual orientation of the molecules (head-to-tail) imprinted into their supramolecular connectivity. The latter one exists in the form of flat four-connected network (similar to the network in the structure of **3**) and the orientation of all integrated molecular dipoles is concerted and additive (Fig. S7). Thus the polar hydrogen bonded layer is generated, although bulk polarity of the entire structure is eliminated by anti-alignment of the polarities from successive layers (Fig. S8). Nevertheless, the hydrogen bonding scheme in **4** could be viewed as important paradigm for the developing of polar crystals.

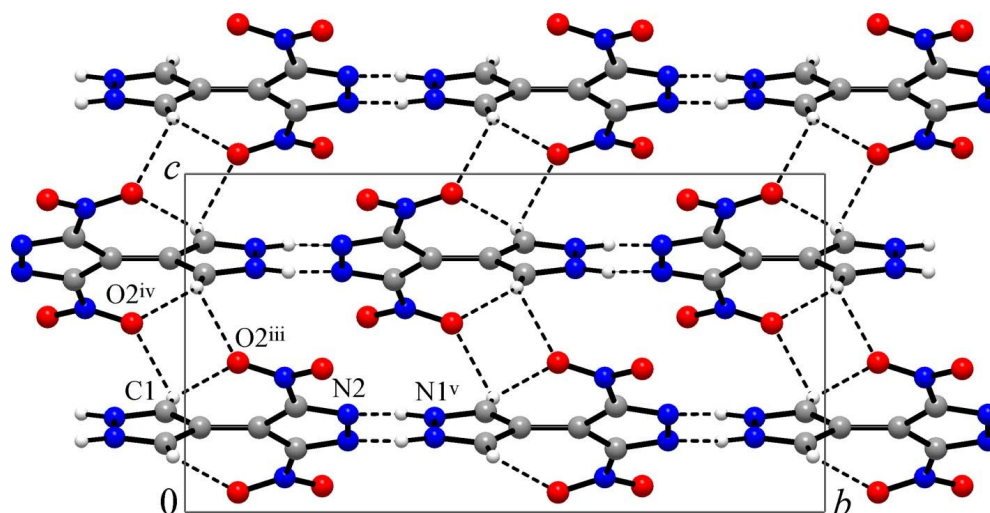


**Figure S8.** The interlayer interactions, bifurcate CH...O bonding, seen in the structure of **4**. Note that the polarity of the successive layers is opposite.

**Table S6.** Hydrogen-bond geometry (Å, °) for structure of 3,5-dinitro-4,4'-bipyrazole **4**.<sup>a)</sup>

Donor (D)	Hydrogen (H)	Acceptor (A) <sup>a)</sup>	D-H	H...A	D...A	∠DH...A
N1	H1N	N2 <sup>ii</sup>	0.97(2)	1.89(2)	2.8410(14)	165.4(19)
N1	H1N	O1 <sup>ii</sup>	0.97(2)	2.45(2)	3.0522(13)	120.2(16)
C1	H1	O2 <sup>iii</sup>	0.951(17)	2.652(17)	3.5292(16)	153.7(12)
C1	H1	O2 <sup>iv</sup>	0.951(17)	2.742(16)	3.5093(17)	138.3(12)

<sup>a)</sup> The bond N1H...N2<sup>ii</sup> is considered as strong and directional; the parameters for N1H...O1<sup>ii</sup> are given for comparison with bifurcate bonding in the structure of **3**. <sup>b)</sup> Symmetry codes: (ii) 0.5-x, -0.5+y, 0.5-z; (iii) 1-x, y, 0.5-z; (iv) x, -y, -0.5+z.

## 2.4. Crystal structure of 3,5,3'-trinitro-4,4'-bipyrazole (**5**)

Supramolecular structure of the compound is very similar to the above layered structures of **3** and **4**. Primary intermolecular linkage is provided by bifurcate NH...N,O hydrogen bonding (Table S7), which connects the molecules to four closest neighbors. It worths noting that the most acidic and polarized NH site of the dinitropyrazole moiety establishes the bond to the most basic of the N-sites (*i.e.* mononitropyrazole) (Fig. S9). For this bond, the effect of bifurcation is only very minor, and the branch to nitro-O acceptor is very weak (if present) as may be found from comparison of N1...N4<sup>i</sup> and N1... O5<sup>i</sup> separations (2.877(2), 3.107(2) Å, respectively) and N1H...N4<sup>i</sup> and N1H...O5<sup>i</sup> bond angles (157(2), 124(2)°, respectively) [symmetry code: (i) -1+x, y, z]. For the second H-bond, nitropyrazole NH donor to dinitropyrazole-N,O acceptor, two branches are comparable, and the N... O5 separation is even shorter (Table S7).

In addition to these stronger hydrogen bonds, the layer comprises also weaker CH $\cdots$ O interactions [C4 $\cdots$ O4<sup>iii</sup> = 3.353(2) Å; Symmetry code: (iii)  $x, 0.5-y, 0.5+z$ ], very similar to **4**. However, with the increased number of the NO<sub>2</sub> groups at the expense of number of the CH groups (**3** to **5**), the CH $\cdots$ O bond network thins out and, instead of the hydrogen bonds present in **3**, short  $\pi$ -hole/lone pair between the adjacent NO<sub>2</sub> groups are generated [N $\cdots$ O = 2.947(2) Å, See Fig. S9]. That the overall supramolecular structure actually remains intact under such a substitution, suggests comparable energetics and steric demands for these two kinds of interactions. Recently we have illustrated such inheritance of the motifs sustained by CH $\cdots$ O and  $\pi$ -hole/lone pair NO<sub>2</sub>/NO<sub>2</sub> bonding, for a series of non-covalent frameworks formed by 1,4-dinitrobutadienes.<sup>[S17]</sup> The layers in the structure of **5** pack in the *ac* plane and weak interlayer interactions are provided by a second branch of bifurcate CH $\cdots$ O bond [C4 $\cdots$ O2<sup>iv</sup> = 3.260(3) Å;  $\angle$  C4H $\cdots$ O2<sup>iv</sup> = 140.4(15)°; Symmetry code: (iv)  $1-x, -y, 1-z$ ]. This pack visualizes clear scheme for evolution of supramolecular patterns in the structures of polynitro-4,4'-bipyrazoles, as depicted in Fig. S10. With the increased number of NO<sub>2</sub> groups and larger molecular twist angle (**2**, **3**  $\rightarrow$  **4**), the flat four-connected nets observed in **2** and **3** experience corrugation yet preserving either dimensionality or topology. Such feature as bent along the chain of the molecules (already accumulated in **5**) is a major step towards disintegration of favorable stack of successive layers. With further increase in a number of NO<sub>2</sub> groups, even larger molecular twist angle (**5**  $\rightarrow$  **6**) and loss of any CH $\cdots$ O bonding, the present array collapses into one-periodic four-connected net, which is described below for the structure of **6**.

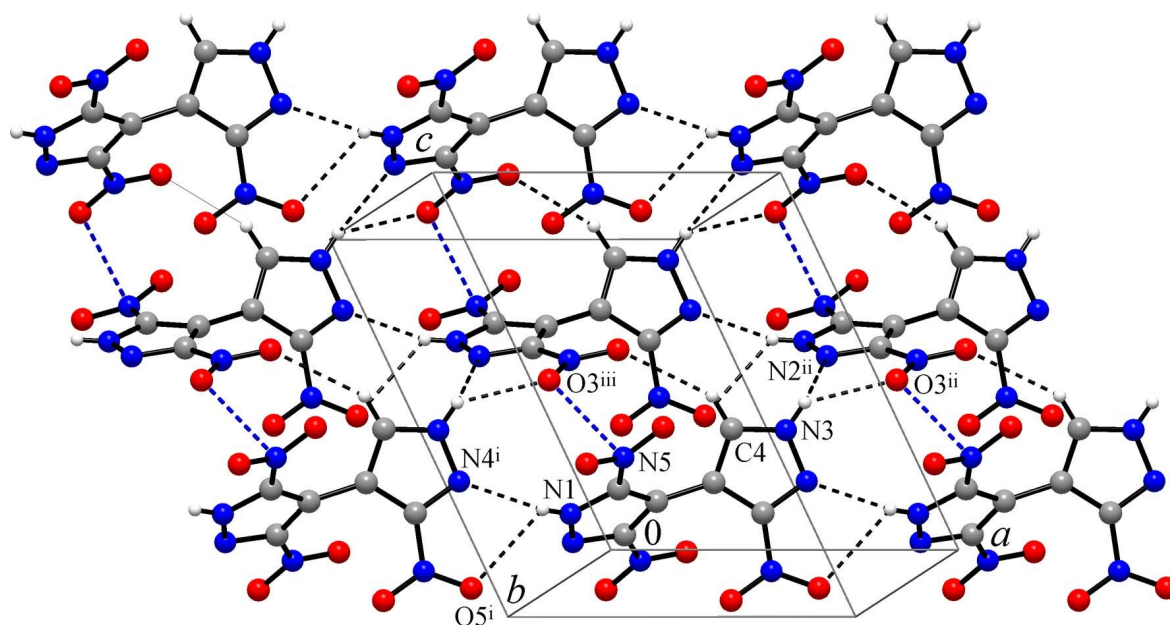


**Figure S9.** Fragment of hydrogen bonded layer in the structure of **5**, with dotted lines indicating H-bonds and intermolecular  $\pi$ -hole/lone pair interactions. [Symmetry codes: (i)  $-1+x, y, z$ ; (ii)  $1+x, 0.5-y, 0.5+z$ ; (iii)  $x, 0.5-y, 0.5+z$ ].

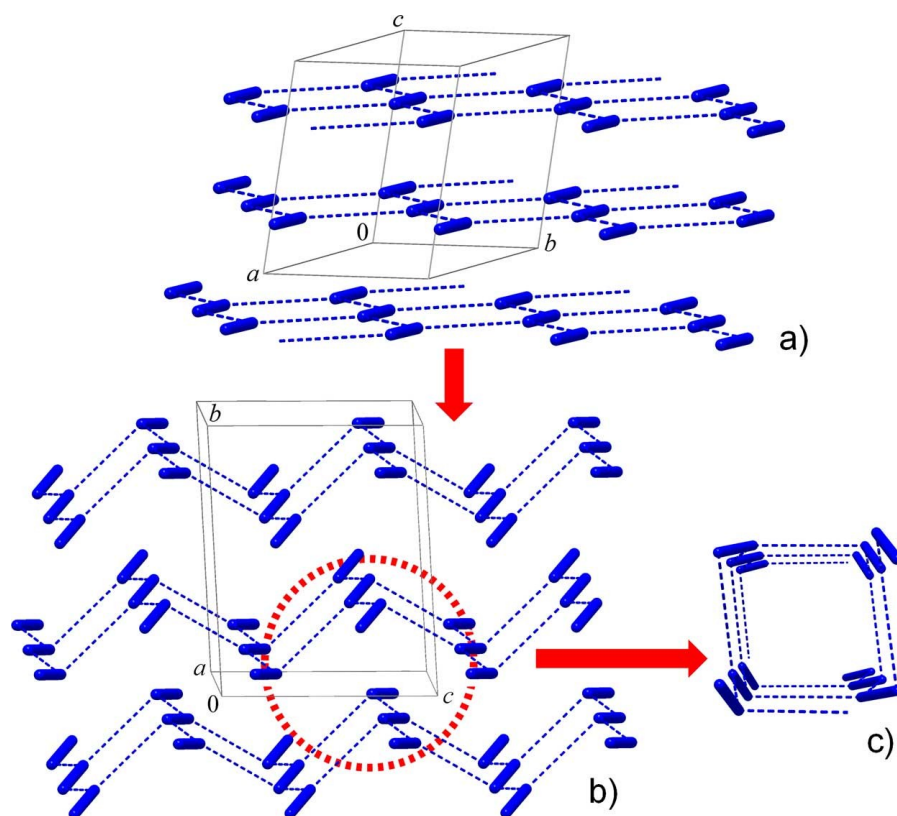


**Figure S10.** Evolution of supramolecular organization of polynitro-4,4'-bipyrazoles (blue sticks represent four-connected molecules and dotted lines refer to principal hydrogen bonding): a) Flat layers in the structures of **3** and **4**; b) Corrugated layers in the structure of **5**; c) One-periodic arrangement in the structure of **6**.

**Table S7.** Hydrogen-bond geometry ( $\text{\AA}$ ,  $^\circ$ ) for structure of 3,3',5-trinitro-4,4'-bipyrazole **5**.

Donor (D)	Hydrogen (H)	Acceptor (A) <sup>a)</sup>	D-H	H...A	D...A	$\angle\text{DH}\cdots\text{A}$
N1	H1N	N4 <sup>i</sup>	0.78(2)	2.15(2)	2.877(2)	157(2)
N1	H1N	O5 <sup>i</sup>	0.78(2)	2.61(2)	3.107(2)	124(2)
N3	H2N	O3 <sup>ii</sup>	0.81(2)	2.33(2)	2.996(2)	138.9(19)
N3	H2N	N2 <sup>ii</sup>	0.81(2)	2.65(2)	3.202(2)	126.2(18)
C4	H4	O4 <sup>iii</sup>	0.93(2)	2.54(2)	3.353(2)	145.8(15)
C4	H4	O2 <sup>iv</sup>	0.93(2)	2.49(2)	3.260(3)	140.4(15)

<sup>a)</sup> Symmetry codes: (i)  $-1+x, y, z$ ; (ii)  $1+x, 0.5-y, 0.5+z$ ; (iii)  $x, 0.5-y, 0.5+z$ ; (iv)  $1-x, -y, 1-z$ .

## 2.5. Crystal structure of 3,5,3',5'-tetranitro-4,4'-bipyrazole (**6**)

The compound crystallizes in a tetragonal space group  $P4_2/n$  and it exhibits very original supramolecular structure, while providing further evolution of general trends observed for **2-5**. In particular, interactions with the nitro oxygen atoms appear to be most crucial for organization of

hydrogen bonded framework, while bonding to pyrazole N-acceptor is present only as a less directional branch of bifurcate NH...O,N bond [ $\angle \text{N3H}\cdots\text{O3}^{\text{ii}} = 166.4(18)^\circ$  vs.  $\angle \text{N3H}\cdots\text{N2}^{\text{ii}} = 124.7(16)^\circ$ ; symmetry code: (ii)  $x, y, -1+z$ ]. This indicates weak basicity of pyrazole-N atoms and their less steric accessibility.

As may be compared to **5**, with a larger twist angle imposed by the molecular frame and loss of interlayer CH...O linkage, the 2D array of H-bonded molecules collapses forming supramolecular tubes, *i.e.* one-periodic 2D structure. First, the strongest and very directional bonds N1H... O8<sup>i</sup> [ $\text{N}\cdots\text{O} = 2.8457(14) \text{ \AA}$ ;  $\angle \text{NH}\cdots\text{O} = 171.7(16)^\circ$ ; symmetry code: (i)  $y, 0.5-x, 0.5-z$ ] assemble the molecules into tetramers, possessing shape of the figure eight (Fig. S11). Second, weaker bifurcate bonding of the second pyrazole NH-donor donor (Table S8) itself leads to a connection of the molecules into linear chains along *c* axis (within the chain the molecules are related by a simple translation). With this bifurcate hydrogen bonding, the tetramers shown in Fig. S11 aggregate forming supramolecular tubes down the *c* axis (See Fig. S12 and Fig. 3 of the main text).

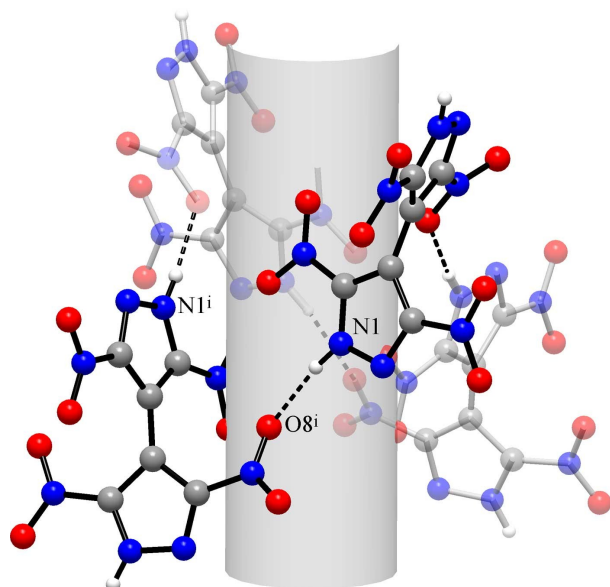


**Figure S11.** Structure of **6**: A finite arrangement of four molecules, in the form of figure eight, which is maintained by a set of strongest hydrogen bonds N1H... O8<sup>i</sup> [Symmetry code: (i)  $y, 0.5-x, 0.5-z$ ].

With a total elimination of competitive CH...O and stacking interactions seen in **2-5**, the role of nitro groups becomes crucial even beyond the hydrogen bonding: in total twelve short  $\pi$ -hole/lone pair N...O contacts (with a cut-off limit of 3.25  $\text{\AA}$ ) of NO<sub>2</sub>/NO<sub>2</sub> and NO<sub>2</sub>/pyrazole types contribute to the dense packing. The shortest nitro/nitro contacts in the structure of **6** [ $\text{N8}\cdots\text{O2}^{\text{iv}} = 2.9115(15) \text{ \AA}$ ; symmetry code (iv)  $0.5-y, x, -0.5-z$ ] (Fig. S13) approach the parameters of strongest NO<sub>2</sub>/NO<sub>2</sub> interactions observed in the structure of the energetic material heptanitrocubane (2.80  $\text{\AA}$ ).<sup>[S18]</sup> These contacts constitute the most notable environment of the N8O7O8 group, which supports interactions at both axial sides simultaneously (Fig. S13, a).

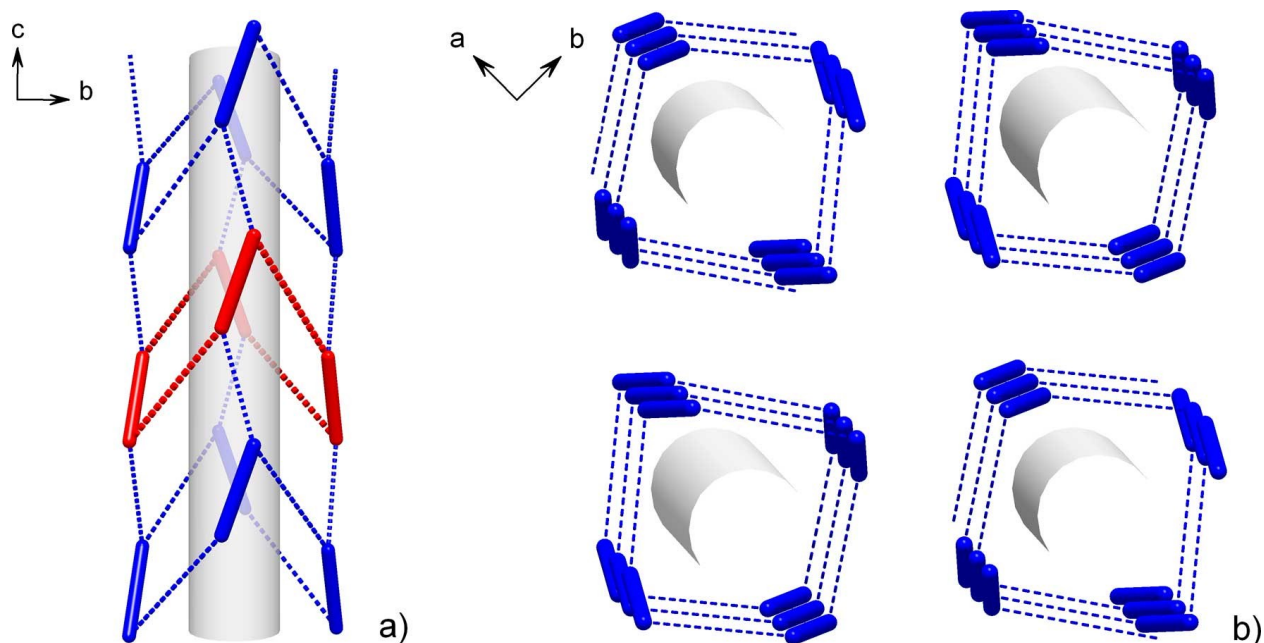


**Figure S12.** A schematic representation of the structure of **6** (the bipyrzole molecules are shown as sticks and their hydrogen bonding to four closest neighbors as dotted lines): a) Supramolecular tubes running down *c* axis. The tetramer presented in the previous figure is marked in red. b) View down the *c* direction, showing packing of four neighboring tubes.

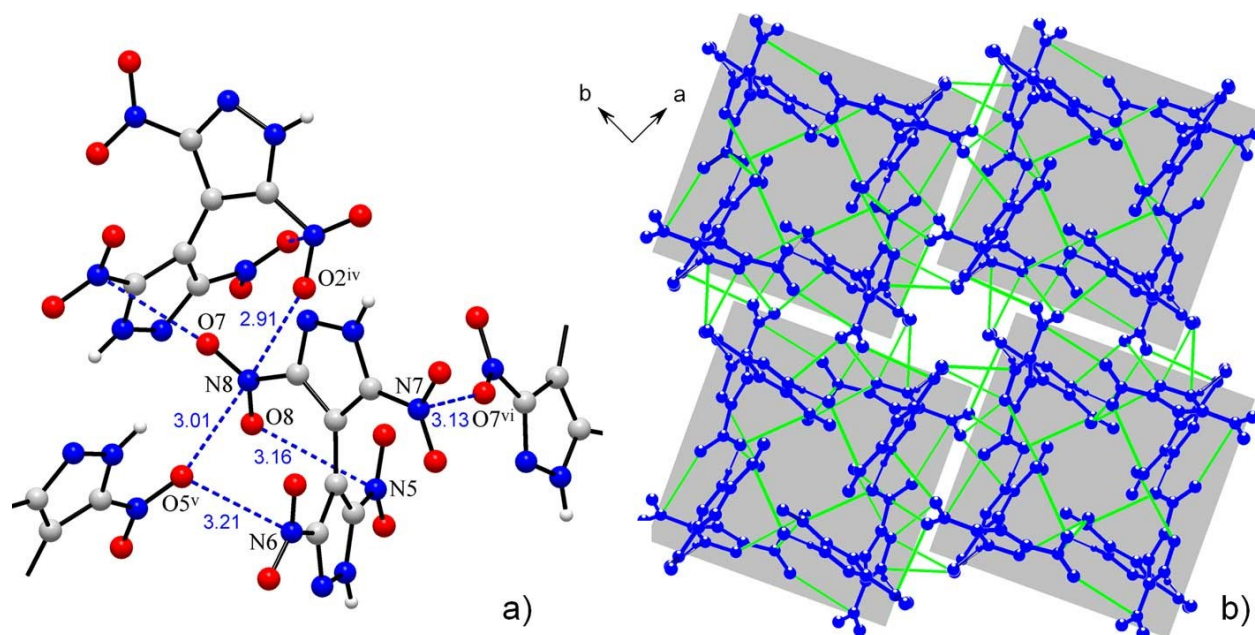


**Figure S13.** a) Short N...O (nitro/nitro) contacts in the structure of **6**, which are marked with dotted lines; b) Significance of  $\pi$ -hole/lone pair interactions for the packing of **6**: Grey squares distinguish supramolecular tubes and green lines indicate the arising short N...O contacts (cut-off limit is 3.25 Å), either of nitro/nitro or nitro/pyrazole types [Symmetry codes (iv)  $0.5-y, x, -0.5-z$ ; (v)  $0.5+y, -x, 0.5+z$ ; (vi)  $y, 0.5-x, -0.5-z$ ].

**Table S8.** Hydrogen-bond geometry (Å, °) for structure of 3,5,3',5'-tetranitro-4,4'-bipyrazole **6**.

Donor (D)	Hydrogen (H)	Acceptor (A) <sup>a)</sup>	D-H	H...A	D...A	∠DH...A
N1	H1N	O8 <sup>i</sup>	0.904(18)	1.949(18)	2.8457(14)	171.7(16)
N3	H2N	O3 <sup>ii</sup>	0.87(2)	2.33(2)	3.1849(16)	166.4(18)
N3	H2N	N2 <sup>ii</sup>	0.87(2)	2.418(19)	3.0027(15)	124.7(16)

<sup>a)</sup> Symmetry codes: (i)  $y, 0.5-x, 0.5-z$ ; (ii)  $x, y, -1+z$ .

## 2.6. Crystal structure of 3,5,3',5'-tetranitro-4,4'-bipyrazole hydrate **6**·H<sub>2</sub>O

Formation of this molecular adduct dominates isolation and purification of **6** from aqueous solutions and a variety of wet solvents. The hydrate possesses higher packing index [73.6%] and slightly higher density [1.857 g cm<sup>-3</sup>] than the unhydrous material [72.2% and 1.847 g cm<sup>-3</sup>], which is suggestive for stronger intermolecular interactions. Thus, the acidic dinitropyrazole moiety is a very strong donor, but only weak acceptor for conventional H-bonding and therefore one can rationalize benefit from the formation of NH...O bonds with appropriate guests rather than the weaker NH...O interactions with nitro-groups. This factor could be favorable for crystallization of molecular adducts incorporating **6**.

In fact, the role of water molecules is crucial for sustaining the entire supramolecular structure, as revealed by evolution of the hydrogen bonding patterns from **6** to **6** · H<sub>2</sub>O. The weak interactions involving pyrazole and nitro-O acceptors are eliminated at all. Instead, one strong and directional bond to O1w atom [N1...O1w<sup>i</sup> = 2.6470(16) Å; ∠N1H...O1w<sup>i</sup> = 176.2(18)°; Symmetry code: (i)  $-1+x, y, z$ ]

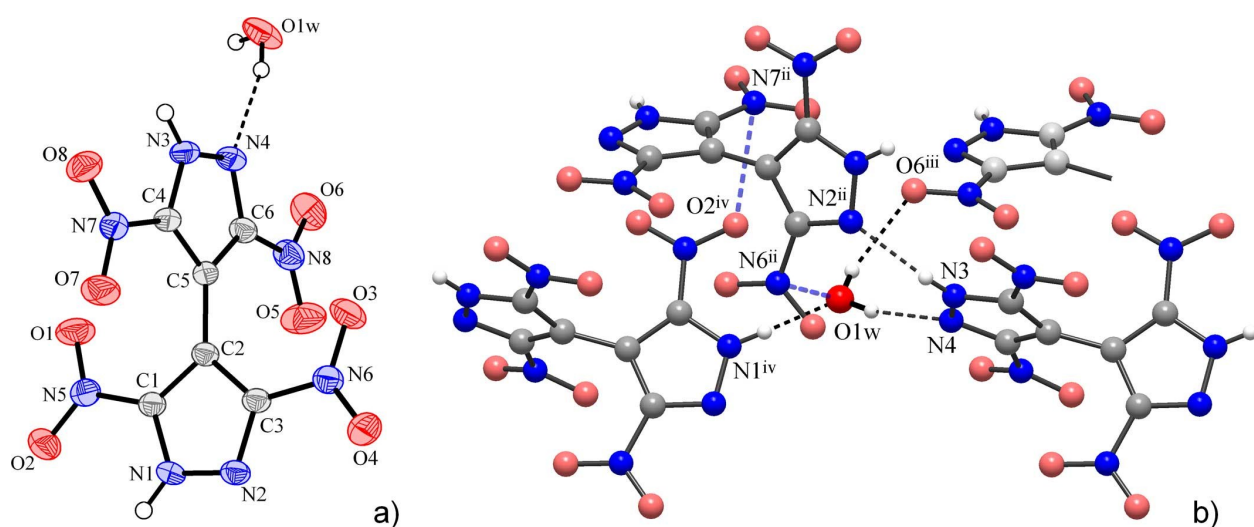


**Figure S14.** a) Molecular structure of **6**·H<sub>2</sub>O showing the atom labeling scheme and thermal ellipsoids drawn at 50% probability level; b) Structural role of water molecule, which establishes three directional H-bonds and one short  $\pi$ -hole/lone pair contact [N(nitro)...OH<sub>2</sub> = 3.058(2) Å].

(Fig. S14) is established and, although the second NH group still secures bonding to the adjacent pyrazole acceptor, the bifurcation of this interaction (compare with the one present in **5**) disappears. As a result, relatively short and directional N3H...N2<sup>ii</sup> bonds are formed [Symmetry code: 0.5+x, 0.5-y, -0.5+z] (Table S9) and these bonds connect the bipyrazole molecules into linear chains (Fig. S15).

Such chains are the clearly distinguishable common motif for both the structures, **6** or **6** · H<sub>2</sub>O. The water molecules unite the chains into the slightly corrugated layers parallel to the *ac* plane, while providing “extended bridges” between the pyrazole-NH and pyrazole-N sites [NH...OH...N]. The only remaining OH hydrogen bond donor is used for interlayer linkage, which involves the nitro-O acceptor [O1w...O6<sup>iii</sup> = 2.9300(18) Å; ∠ O1wH...O6<sup>iii</sup> = 146(2)°; Symmetry code: (iii) *x*, -*y*, -0.5+z]. Thus the entire hydrogen bonded structure represents 3D framework of complex (and new) topology. When considering the bipyrazole (linked to two bipyrazoles and three water molecules) and water (linked to three bipyrazoles) molecules as the net nodes, the three- and five- coordinated binodal net with a point (Schläfli) symbol {6<sup>3</sup>} {6<sup>7</sup>.8<sup>3</sup>} is found.

However, the role of water molecule is important even beyond the conventional hydrogen bonding. In the environment of multiple nitro groups, in addition to the above bonds, it adopts relatively short π-hole/lone pair contact with nitro-N acceptor [N(nitro)...OH<sub>2</sub> = 3.058(2) Å], which completes nearly tetrahedral environment of O1w (N1<sup>iv</sup>, N4, O6<sup>iii</sup> and N6<sup>ii</sup>, see Fig. S14b). Therefore the aqua guest exactly follows the trend for generation of multiple π-hole/lone pair interactions, as already mentioned for structures of **5** and **6**. As may be compared with a latter example, significance of such interactions in **6** · H<sub>2</sub>O is slightly diminished in a favor of more competitive conventional hydrogen bonding. However, the pack still generates nine short N...O contacts (with a cut-off limit of 3.25 Å) corresponding to the NO<sub>2</sub>...NO<sub>2</sub>, NO<sub>2</sub>...pyrazole and H<sub>2</sub>O...NO<sub>2</sub> types, with a shortest separations found for two interacting nitro groups [N7...O2<sup>v</sup> = 2.9714(18) Å; Symmetry code: (v) 0.5+x, 0.5-y, 0.5+z] (Fig. S14b).

**Table S9.** Hydrogen-bond geometry (Å, °) for structure of **6** · H<sub>2</sub>O.

Donor (D)	Hydrogen (H)	Acceptor (A) <sup>a)</sup>	D-H	H...A	D...A	∠DH...A
N1	H1N	O1W <sup>i</sup>	0.828(18)	1.821(19)	2.6470(16)	176.2(18)
N3	H2N	N2 <sup>ii</sup>	0.85(2)	2.083(19)	2.9058(16)	161.7(17)
O1W	H1W	N4	0.85(3)	2.22(3)	3.0479(16)	166(2)
O1W	H2W	O6 <sup>iii</sup>	0.82(3)	2.21(3)	2.9300(18)	146(2)

<sup>a)</sup> Symmetry codes: (i) -1+x, *y*, *z*; (ii) 0.5+x, 0.5-y, -0.5+z; (iii) *x*, -*y*, -0.5+z.

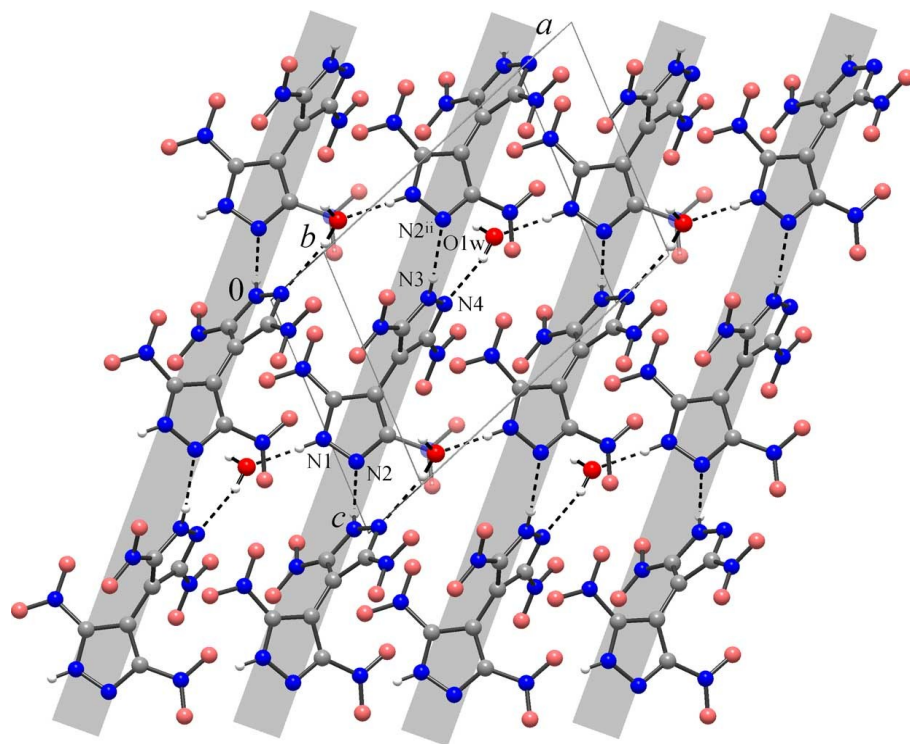


**Figure S15.** Fragment of the structure of  $6 \cdot \text{H}_2\text{O}$ , in a projection nearly to  $ac$  plane: Hydrogen bonded layer comprising chains of  $\text{NH}\cdots\text{N}$  bonded bipyrazole molecules (indicated with grey strips), which are interlinked with water molecules [ $\text{NH}\cdots\text{OH}\cdots\text{N}$ ].

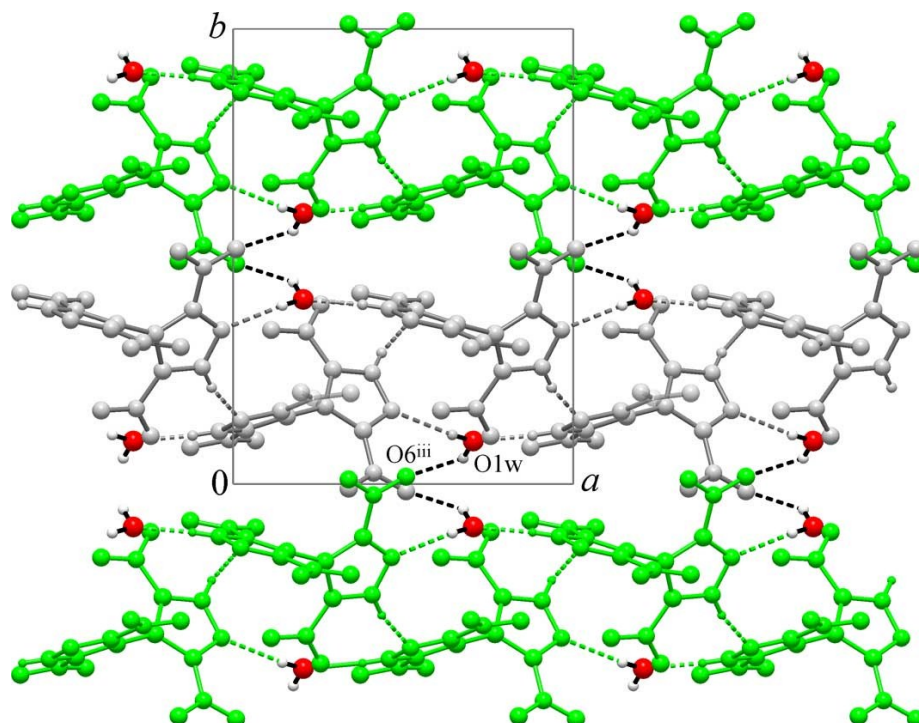


**Figure S16.** Projection of the structure of  $6 \cdot \text{H}_2\text{O}$  on a  $ab$  plane, showing packing of three successive layers (marked in green, grey and green) and interlayer hydrogen bond interactions of water molecules to  $\text{NO}_2$  acceptors [Symmetry code: (iii)  $x, -y, -0.5+z$ .]

### 3. Computations

All calculations were carried out using the Gaussian G09W (revision A.02) program package.<sup>[S19]</sup> The enthalpies (H), were calculated using the complete basis set (CBS) method of Petersson and coworkers. The CBS models use the known asymptotic convergence of pair natural orbital expressions to extrapolate from calculations using a finite basis set to the estimated complete basis set limit. CBS-4 begins with a HF/3-21G(d) structure optimization and the zero-point energy computation. Subsequently, applying a larger basis set a base energy is computed. A MP2/6-31+G calculation with a CBS extrapolation gives the perturbation-theory corrected energy (takes the electron correlation into account). A MP4(SDQ)/6-31+(d,p) calculation is used to correlate higher order contributions. In this study we applied the modified CBS-4M method (M referring to the use of minimal population localization) which is a re-parameterized version of the original CBS-4 method and also includes some additional empirical corrections.<sup>[S20]</sup> The gas-phase enthalpies ( $\Delta_f H^\circ_{(g, M, 298)}$ ) of the species were computed according to the atomization energy method (equation 1).<sup>[S21]</sup>

$$\Delta_f H^\circ_{(g, M, 298)} = H_{(g, M, 298)} - \sum H^\circ_{(g, A_i, 298)} + \sum \Delta_f H^\circ_{(g, A_i, 298)} \quad (1)$$

$\Delta_f H^\circ_{(g, A_i, 298)}$  for the corresponding atoms ( $A_i$ ) were determined experimentally and are reported in the literature while  $H^\circ_{(g, A_i, 298)}$  were calculated theoretically (Table S10).<sup>[S22]</sup>

**Table S10.** CBS-4M electronic enthalpies for atoms C, H, N and O and their literature values for atomic  $\Delta_f H^\circ_{298} / \text{kJ mol}^{-1}$ .

Atom	$-H^{298} / \text{a.u.}$	$\Delta_f H^\circ_{(g, A_i, 298)} [\text{kcal mol}^{-1}]$
H	0.500991	52.103
C	37.786156	171.29
N	54.522462	112.97
O	74.991202	59.56

Standard molar enthalpies of formation were calculated using and the standard molar enthalpies of  $\Delta_f H^\circ_{(g, M, 298)}$  sublimation (estimated using Trouton's rule, equation 2).<sup>[S23]</sup>

$$\Delta_f H^\circ_M = \Delta_f H^\circ_{(g, M, 298)} - \Delta_{sub} H^\circ_M = \Delta_f H^\circ_{(g, M, 298K)} - 188 \cdot T \left[ \frac{\text{J}}{\text{mol}} \right] \quad (2)$$

Where [K] is either the melting point or the decomposition temperature (if no melting occurs prior to decomposition).

The calculation results are summarized in Tables S11.

**Table S11.** Calculation results.

Compound	$-H^{298}$ [a] a.u.	$\Delta_f H^\circ(\text{g,M})$ kJ mol <sup>-1</sup> [b]	$\Delta_f H^\circ(\text{s})$ kJ mol <sup>-1</sup> [c]	$\Delta_f U(\text{s})$ kJ kg <sup>-1</sup> [d]
<b>6</b>	1267.704422	334.0	227.8	796.1
<b>5</b>	1063.413895	333.6	224.9	909.3
<b>4</b>	859.068778	476.5	371.7	1735.9
<b>3</b>	859.126194	325.7	203.5	985.4
<b>2</b>	654.836114	324.1	224.6	1337.0

[a] CBS-4M electronic enthalpy; [b] gas phase enthalpy of formation; [c] standard solid state enthalpy of formation; [d] solid state energy of formation.

### Detonation Parameters

The Chapman-Jouguet (C-J) characteristics, (*i.e.* heat of detonation,  $\Delta EU^\circ$ ; detonation temperature,  $TC\text{-}J$ ; detonation pressure,  $PC\text{-}J$ ; detonation velocity  $VC\text{-}J$ ) based on the calculated  $\Delta_f H^\circ_M$  values, and the theoretical maximum densities were computed using the EXPLO5 V6.03 thermochemical computer code.<sup>[S24]</sup> Calculations for explosives assume ideal behaviour. The estimation of detonation parameters is based on the chemical equilibrium steady-state model of detonation. The Becker-Kistiakowsky-Wilson equation of state (BKW EOS) with the following sets of constants:  $\alpha = 0.5$ ,  $\beta = 0.38$ ,  $\kappa = 9.4$ , and  $\Theta = 4120$  for gaseous detonation products and the Murnaghan equation of state for condensed products (compressible solids and liquids) were applied. The calculation of the equilibrium composition of the detonation products uses modified White, Johnson and Dantzig's free energy minimization technique. The specific energies of explosives ( $f$ ) were calculated according to the ideal gas equation of state assuming isochoric conditions (equation 3).

$$f = p_e \cdot V = n \cdot R \cdot T_c \left[ \frac{\text{kJ}}{\text{molkg}} \right] \quad (3)$$

Where  $p_e$  is the maximum pressure through the explosion,  $V$  is the volume of detonation gases ( $\text{m}^3 \cdot \text{kg}^{-1}$ ),  $n$  is the number of moles of gas formed by the explosion per kilogram of explosive (*Volume*

of Explosive Gases),  $R$  is the ideal gas constant and  $T_c$  is the absolute temperature of the explosion.<sup>[S24,S25]</sup>

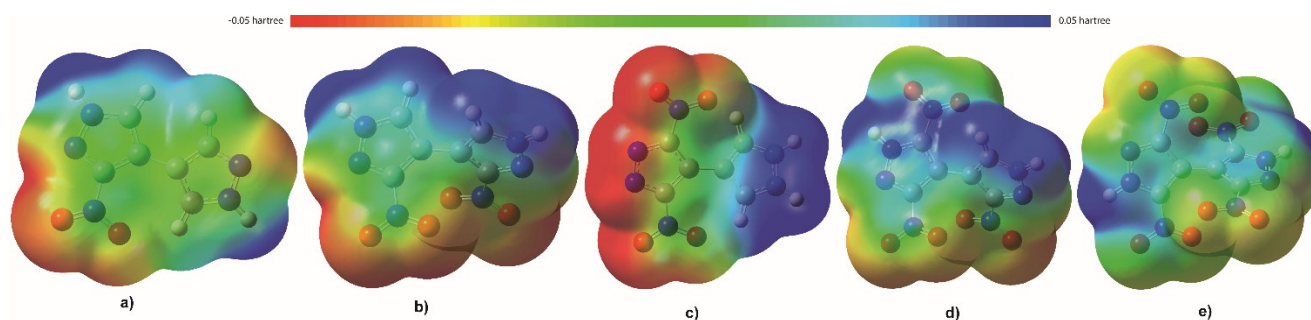


**Figure S17.** Depiction of the calculated [B3LYP/6-31G(d,p)] electrostatic potentials of **2–6** (a:**2**, b:**3**, c:**4**, d:**5**, e:**6**). The 3D isosurface of electron density is shown between  $-0.05$  hartree (electron-rich regions) and  $+0.05$  hartree (electron-poor regions).

### Small-scale shock reactivity test (SSRT)

To evaluate the shock reactivity (explosiveness) of a small-scale shock reactivity test (SSRT) was performed. The SSRT measures the shock reactivity of potentially energetic materials, often below critical diameter, without requiring a transition to detonation.<sup>[26]</sup> The test setup combines the benefits from a lead block test and a gap test. The experimental setup for the small-scale shock reactivity test has been prepared as previously reported in the literature.<sup>[27]</sup> The amount  $ms$  of the was calculated using the following formula:  $ms = V_s \cdot \rho \cdot 0.95$ , (where:  $V_s = 284 \text{ mm}^3$ ). Compounds **5** and **6** were pressed at a consolidation dead load of 3 t with a dwell time of 5 s into a perforated steel block. Neither attenuator (between detonator and sample) nor air gap (between sample and aluminum block) were applied. Initiation of the tested explosive was performed using a commercially available detonator (Orica-DYNADET C2-0ms).

### Thermal stability

Decomposition temperatures were measured *via* differential thermal analysis (DTA) with an OZM Research DTA 552-Ex instrument at a heating rate of  $5 \text{ }^\circ\text{C min}^{-1}$  and in a range of room temperature to  $400 \text{ }^\circ\text{C}$ .

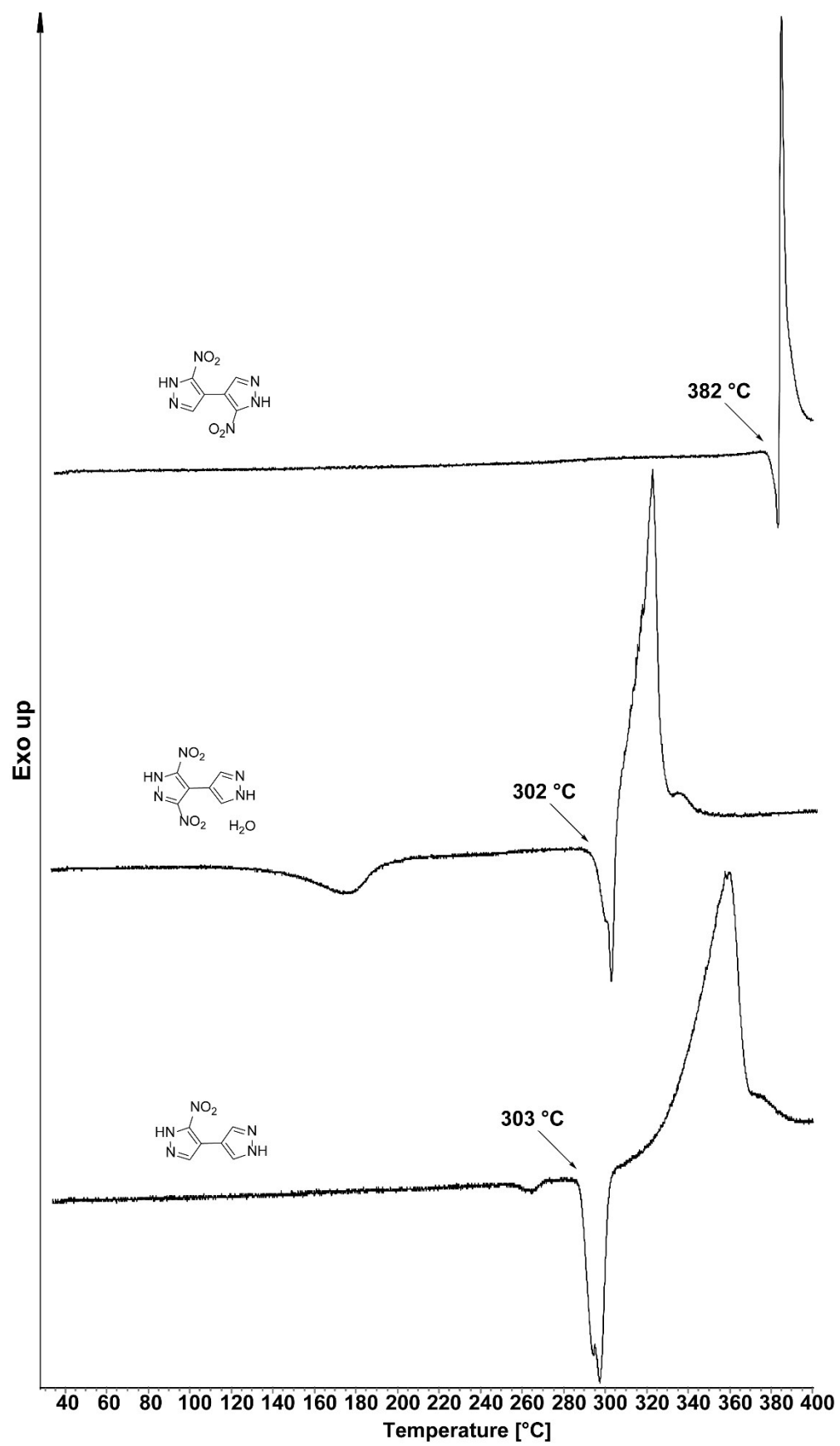


**Figure S18.** DTA plot for compounds 3-nitro-4,4'-bipyrazole (**2**), 3,3'-dinitro-4,4'-bipyrazole (**3**) and 3,5-dinitro-4,4'-bipyrazole monohydrate (**4**·H<sub>2</sub>O).

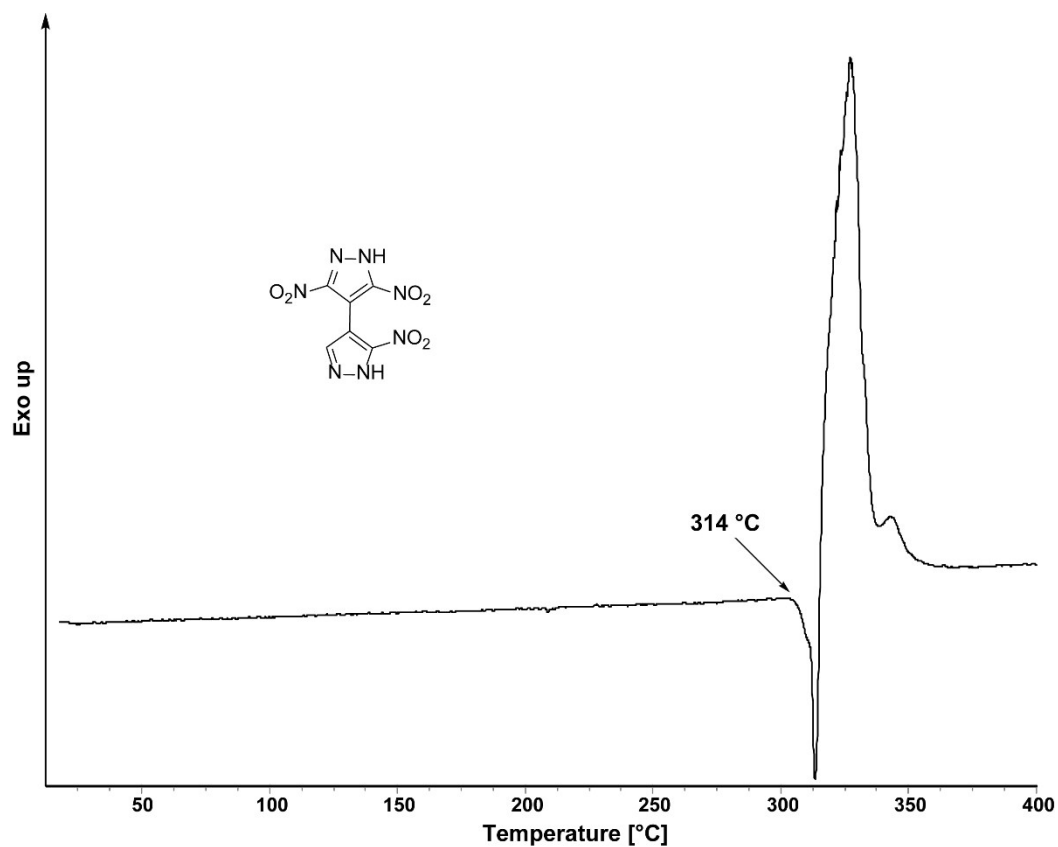


**Figure S22.** DTA plot for compound **5**.

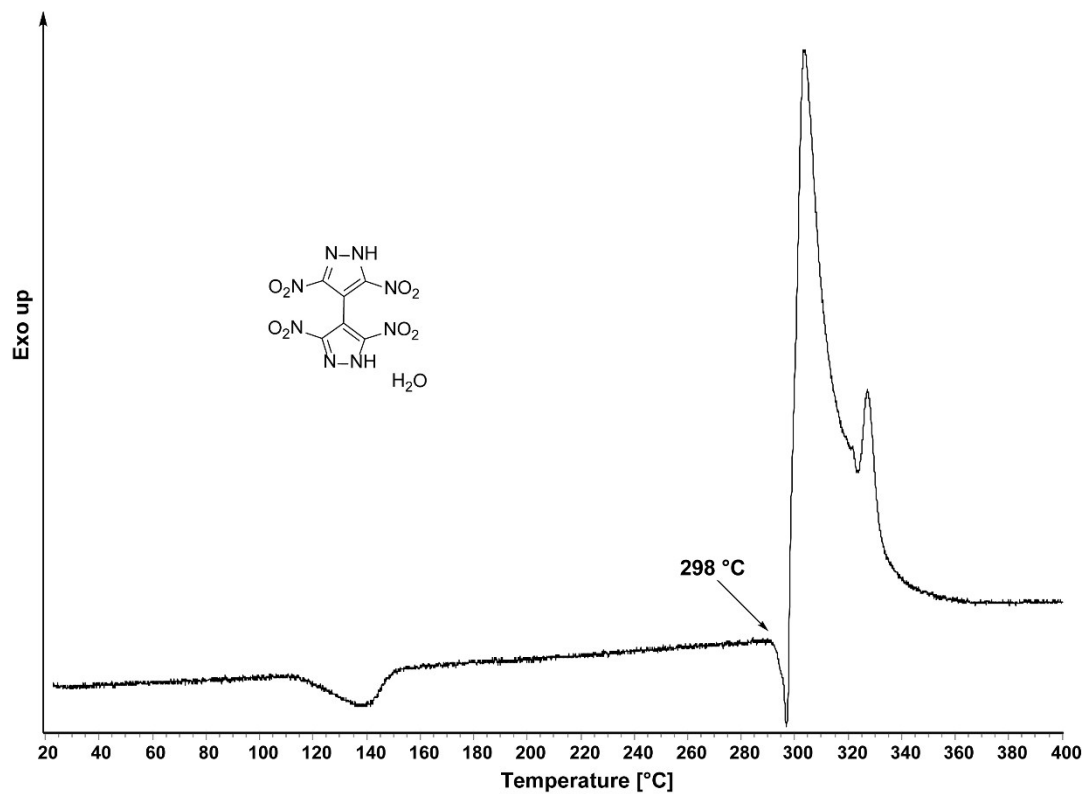


**Figure S19.** DTA plot for compound **6**·H<sub>2</sub>O.

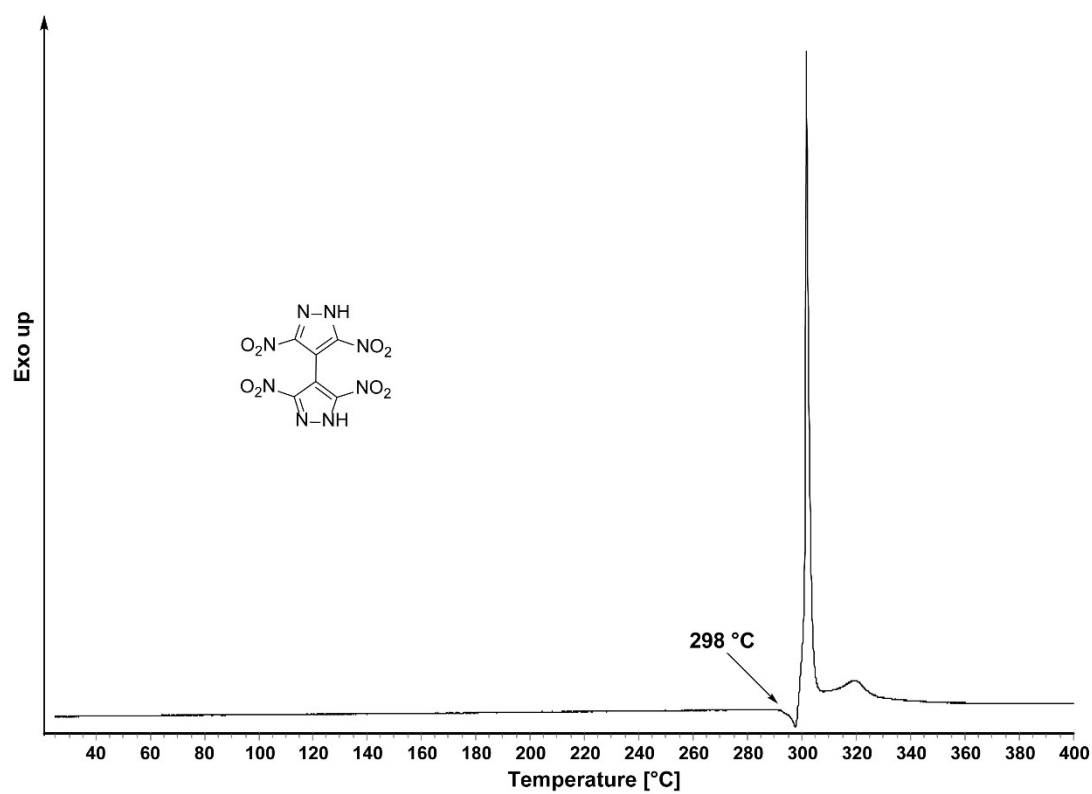


Figure S20. DTA plot for compound 6.

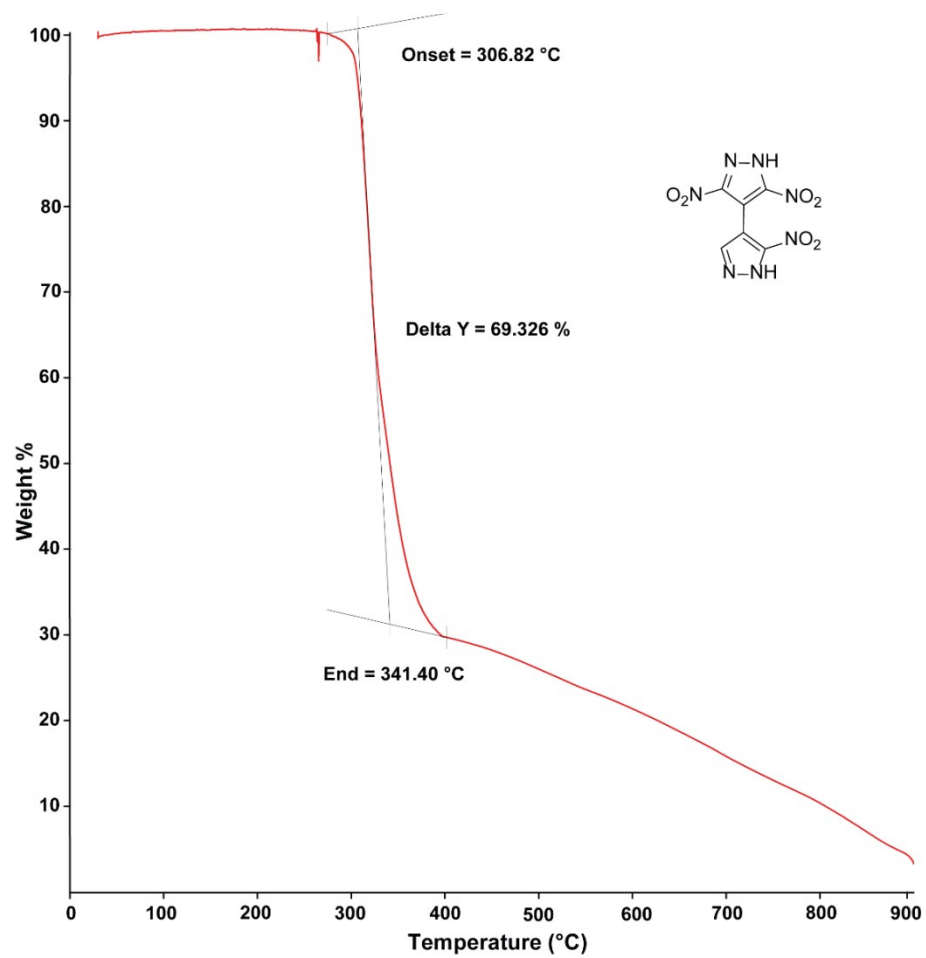
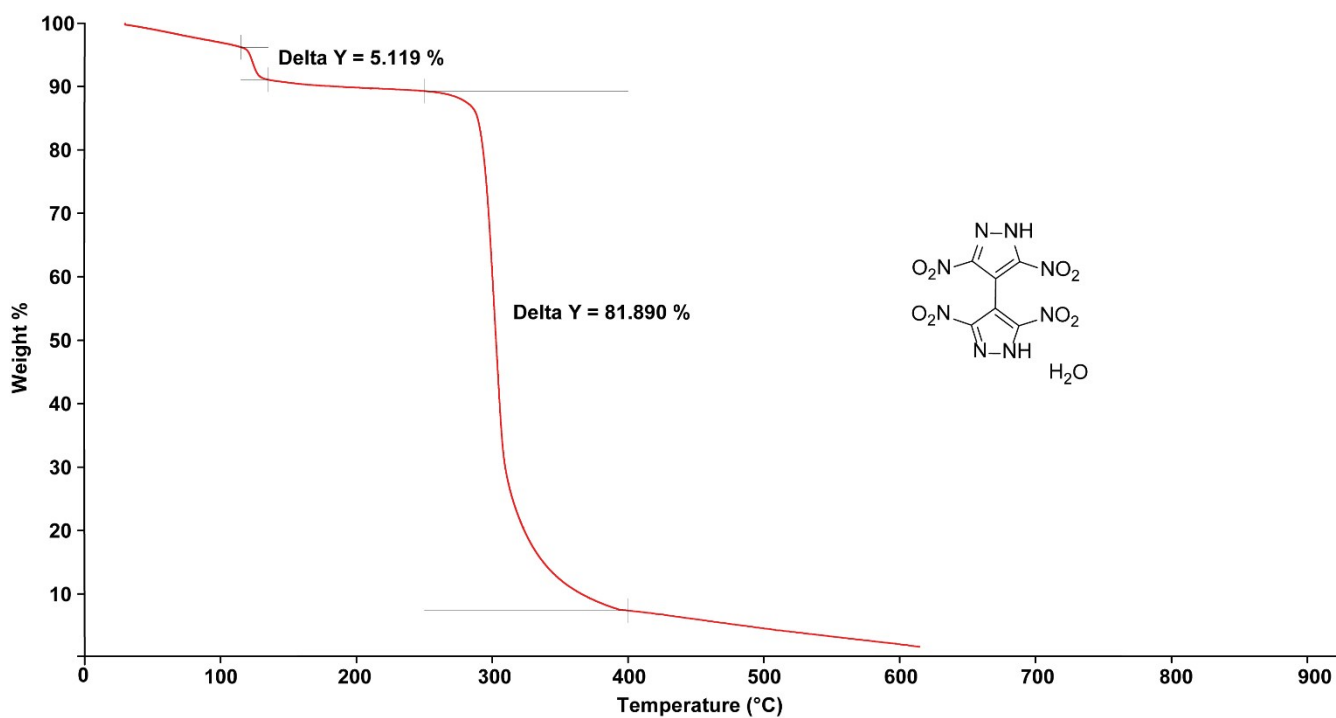
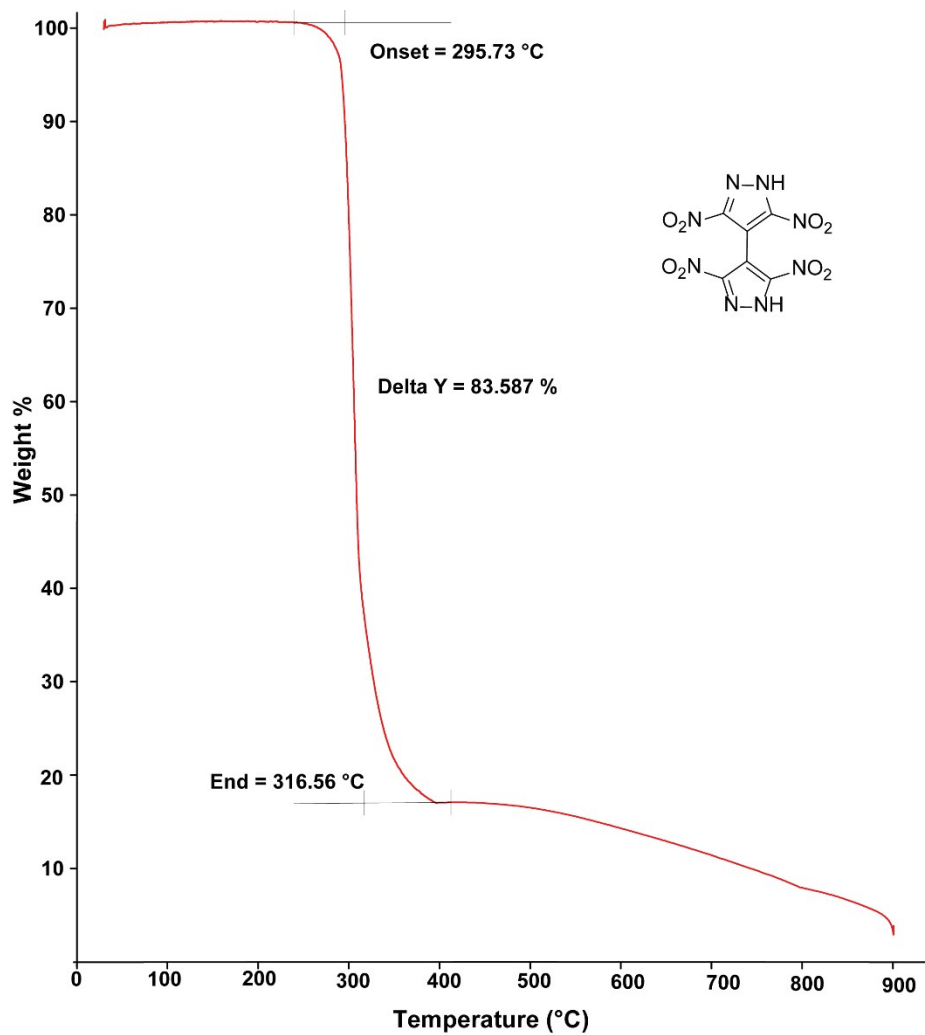


Figure S21. TGA plot for compound 5.



**Figure S22.** TGA plot for compound **6**·H<sub>2</sub>O.



**Figure S23.** TGA plot for compound **6**.

# $^1\text{H}$ and $^{13}\text{C}$ NMR spectra

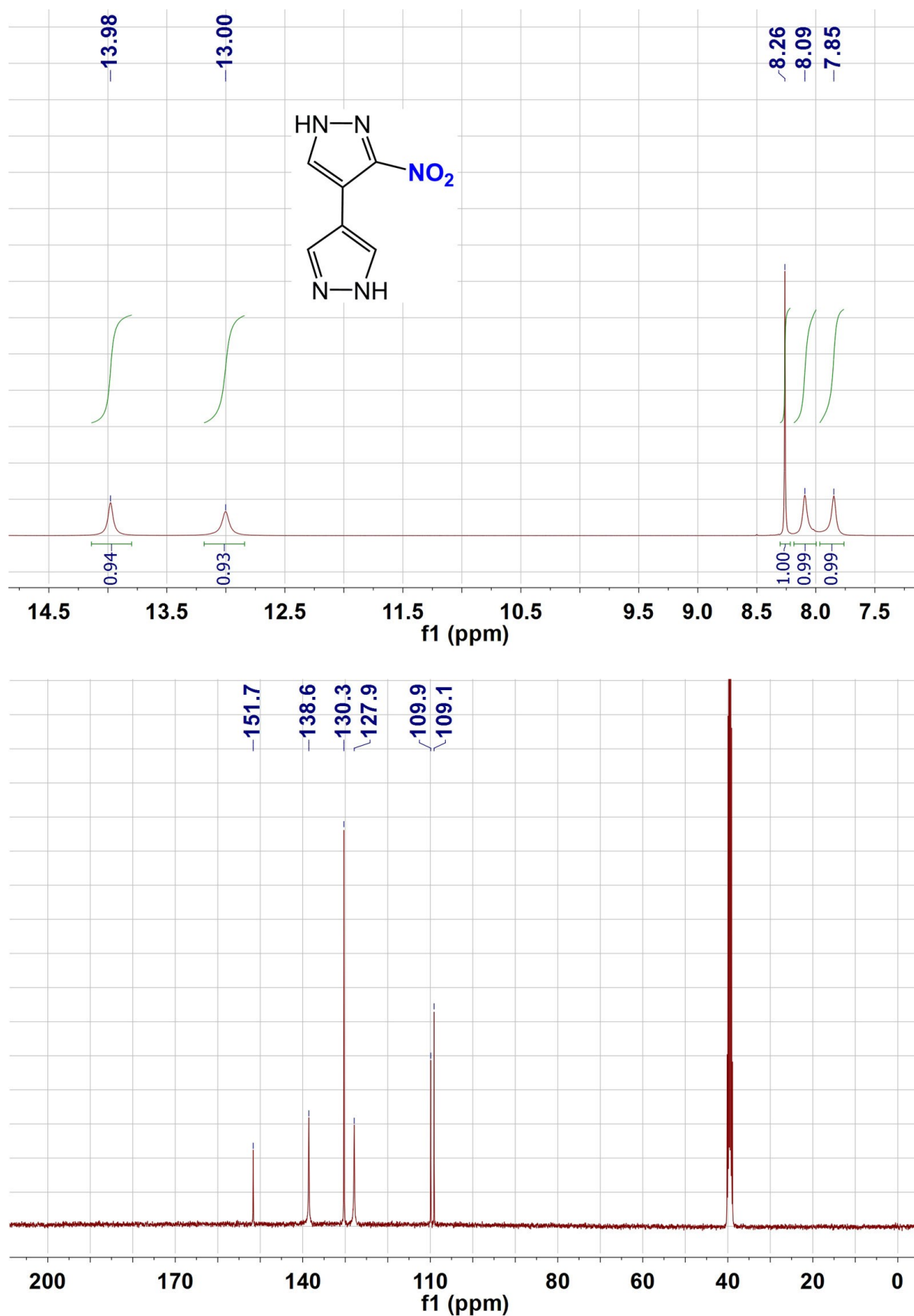


Figure S24.  $^1\text{H}$  and  $^{13}\text{C}$  NMR spectra for 3-nitro-4,4'-bipyrazole (2).

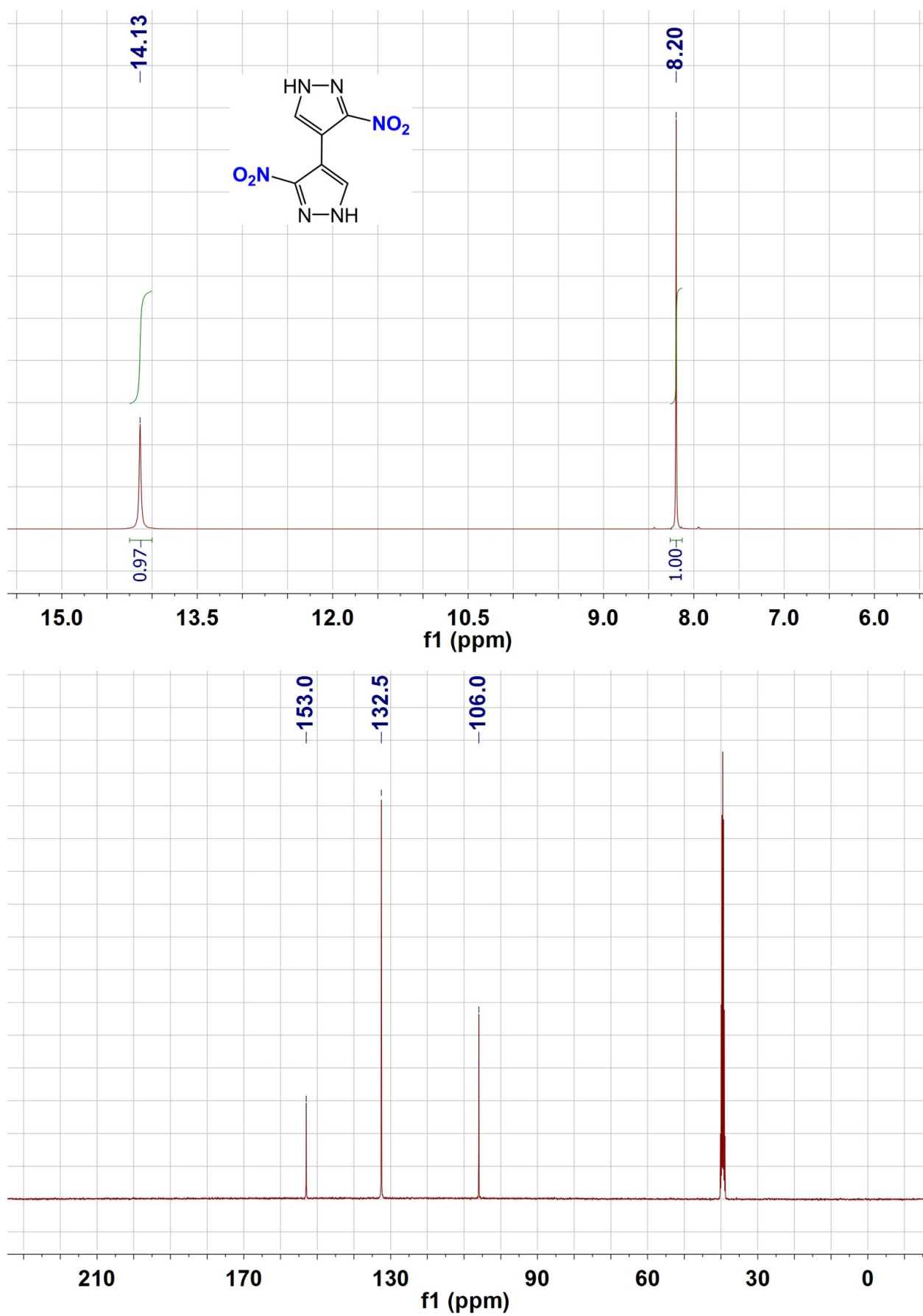


Figure S25.  $^1\text{H}$  and  $^{13}\text{C}$  NMR spectra for 3,3'-dinitro-4,4'-bipyrazole (3).

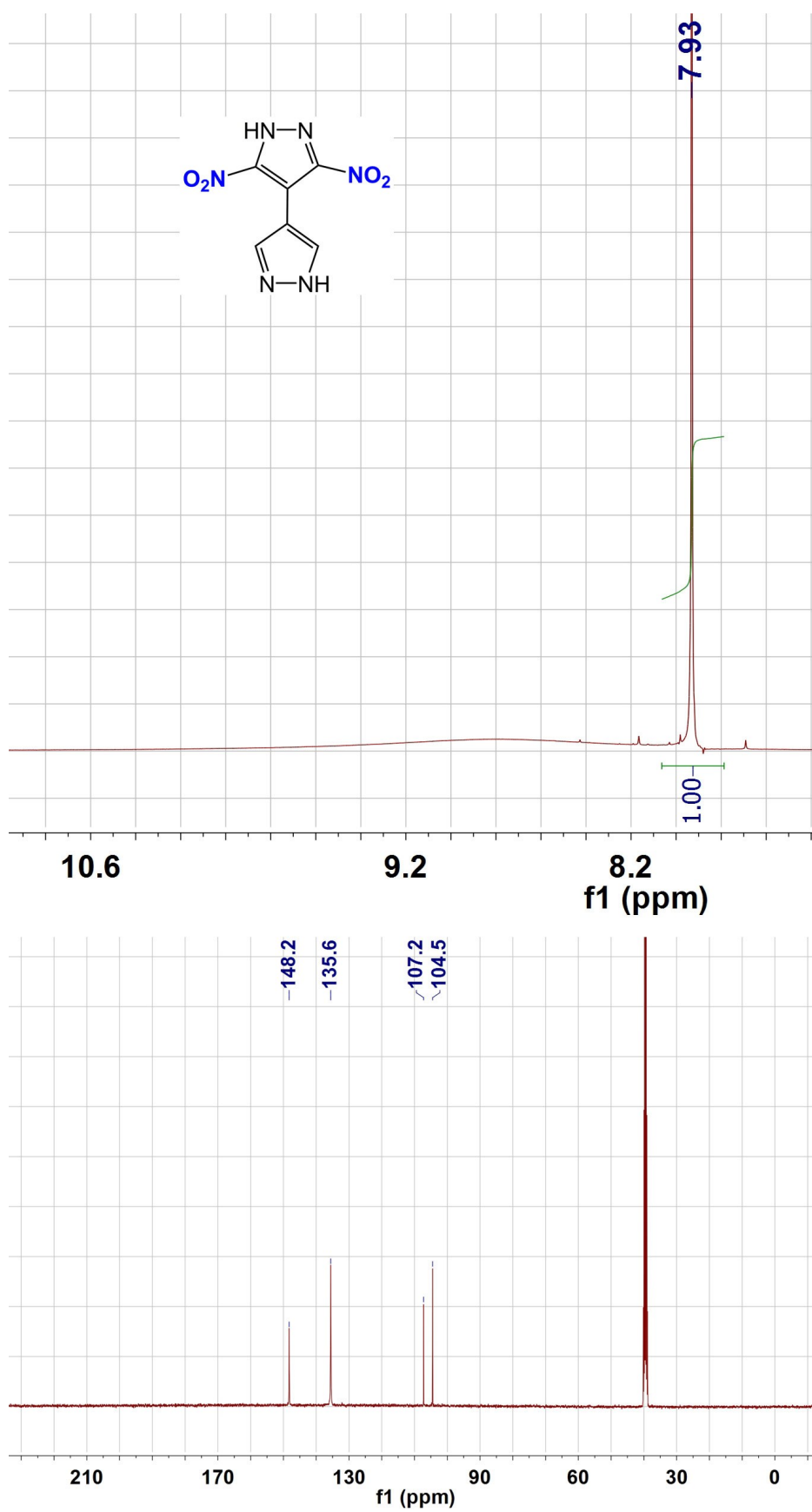


Figure S26. <sup>1</sup>H and <sup>13</sup>C NMR spectra for 3,5-dinitro-4,4'-bipyrazole (4).

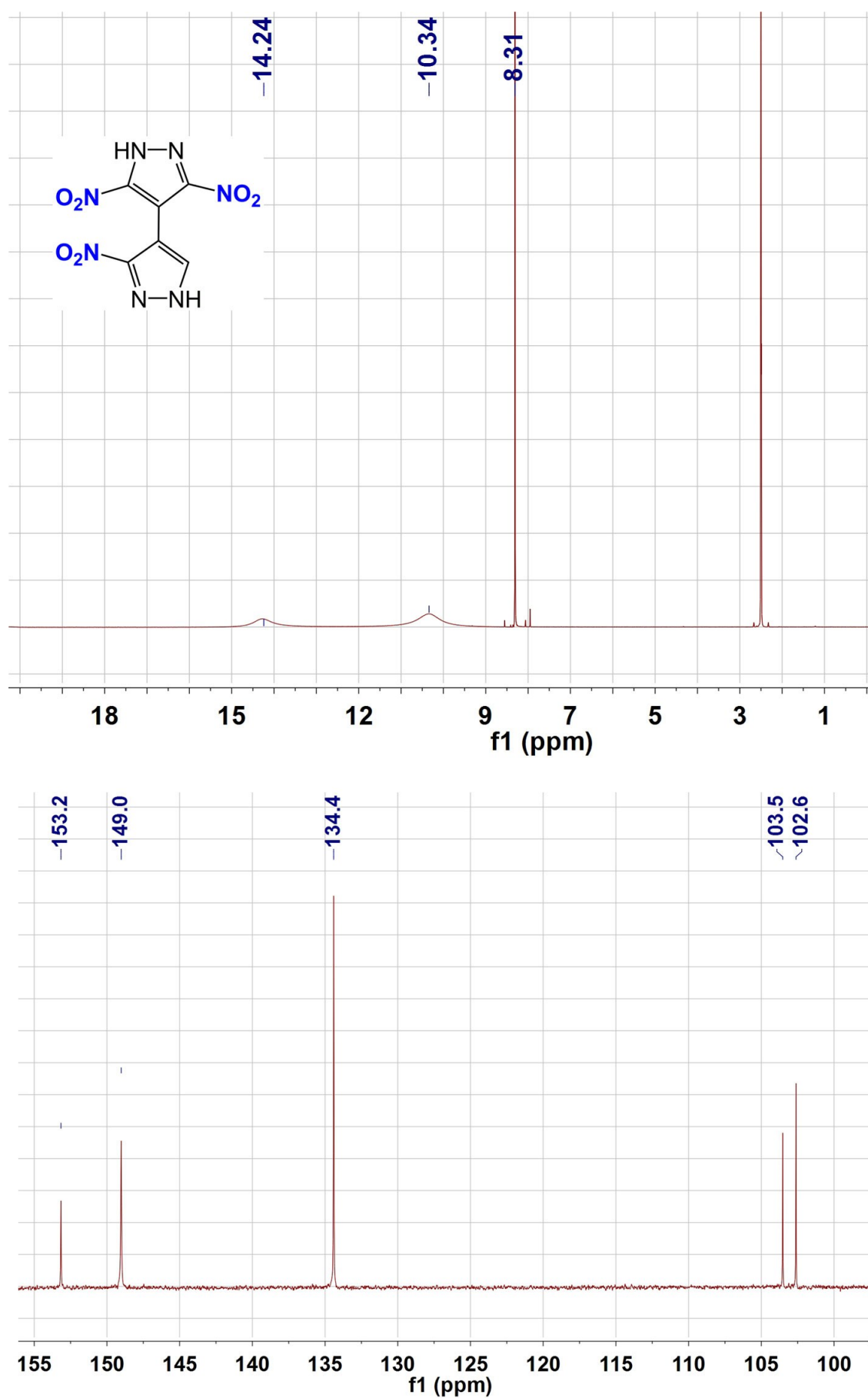


Figure S27. <sup>1</sup>H and <sup>13</sup>C NMR spectra for 3,5,3'-trinitro-4,4'-bipyrazole (5).

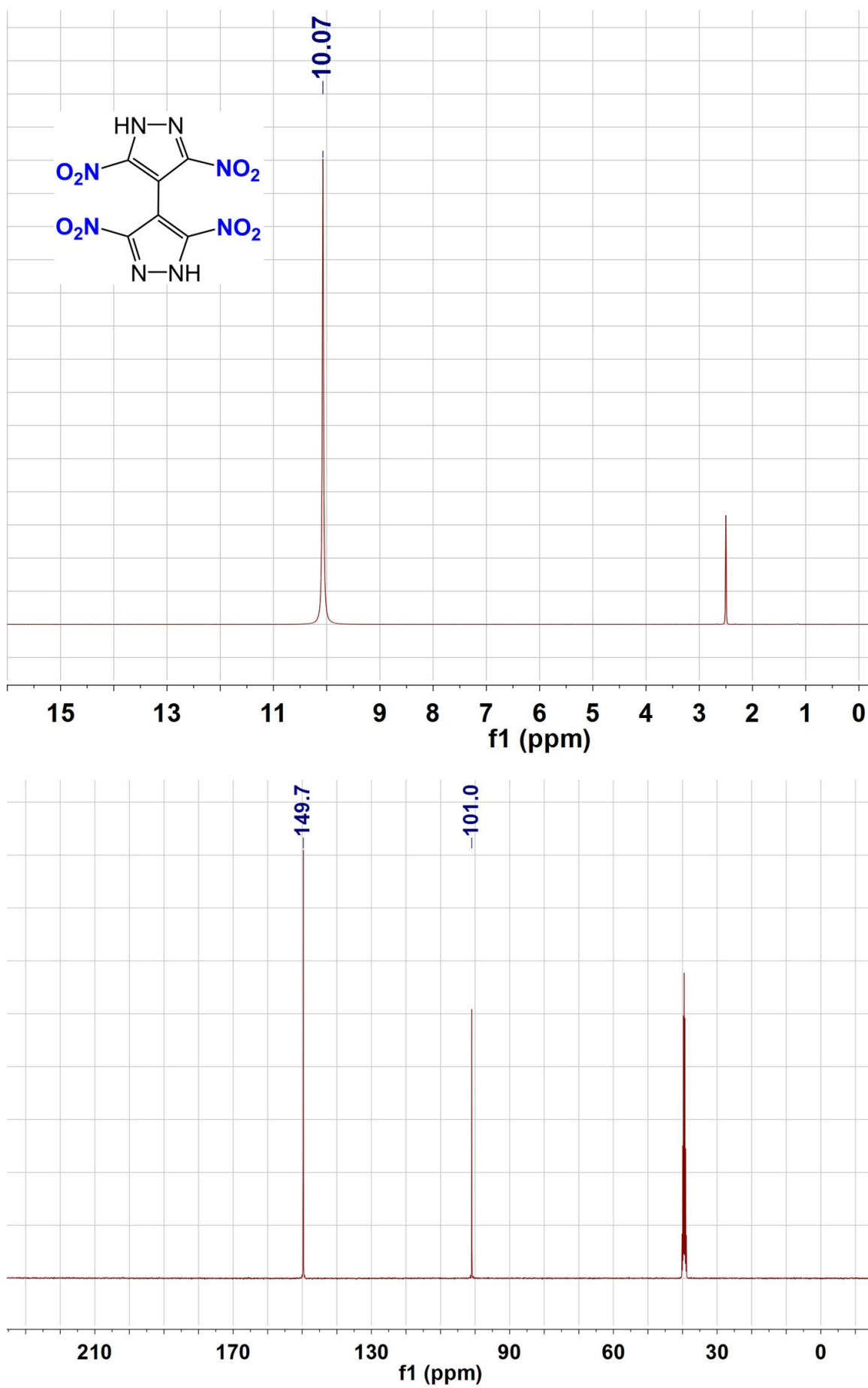


Figure S28.  $^1\text{H}$  and  $^{13}\text{C}$  NMR spectra for 3,5,3',5'-tetranitro-4,4'-bipyrazole (6).

## $^{15}\text{N}$ NMR spectroscopy

$^{15}\text{N}$  NMR (41 MHz,  $d_6$ -DMSO)

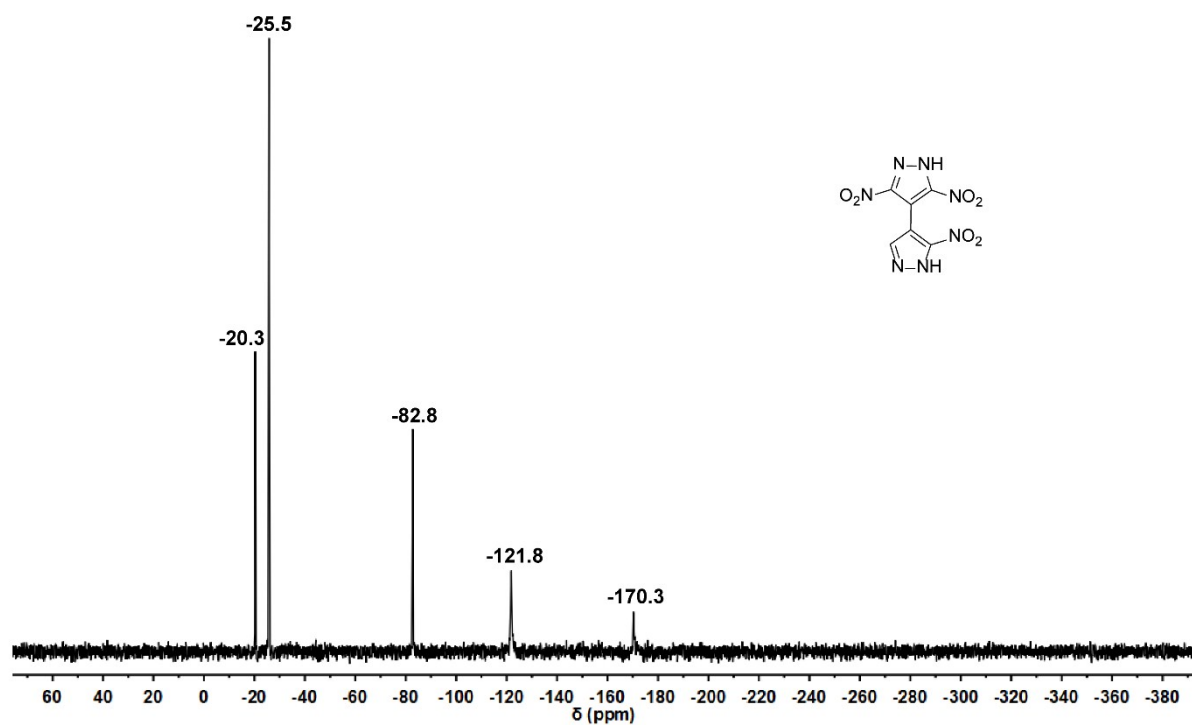


Figure S29.  $^{15}\text{N}$  NMR spectrum of 3,3',5-trinitro-4,4'-bipyrazole (5).

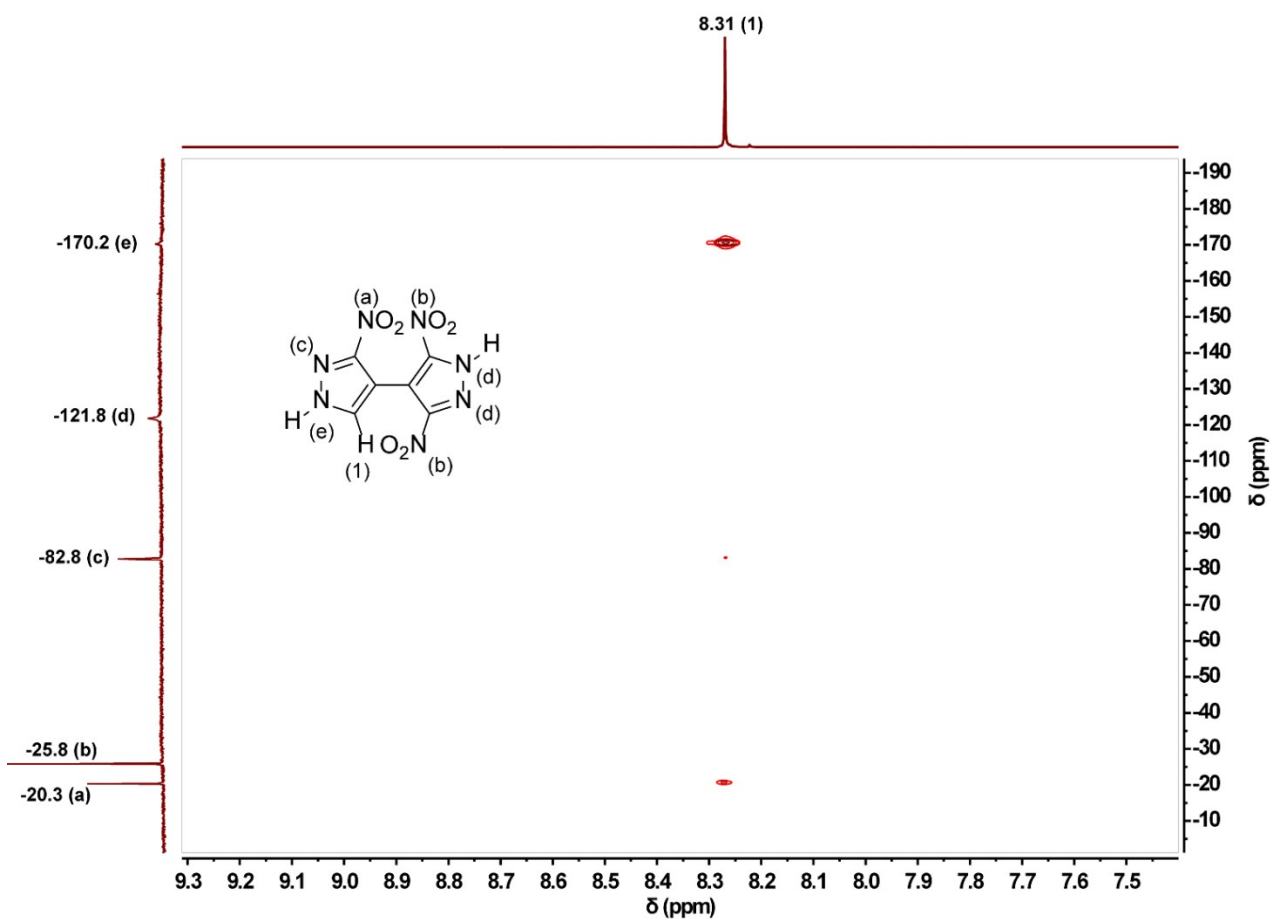
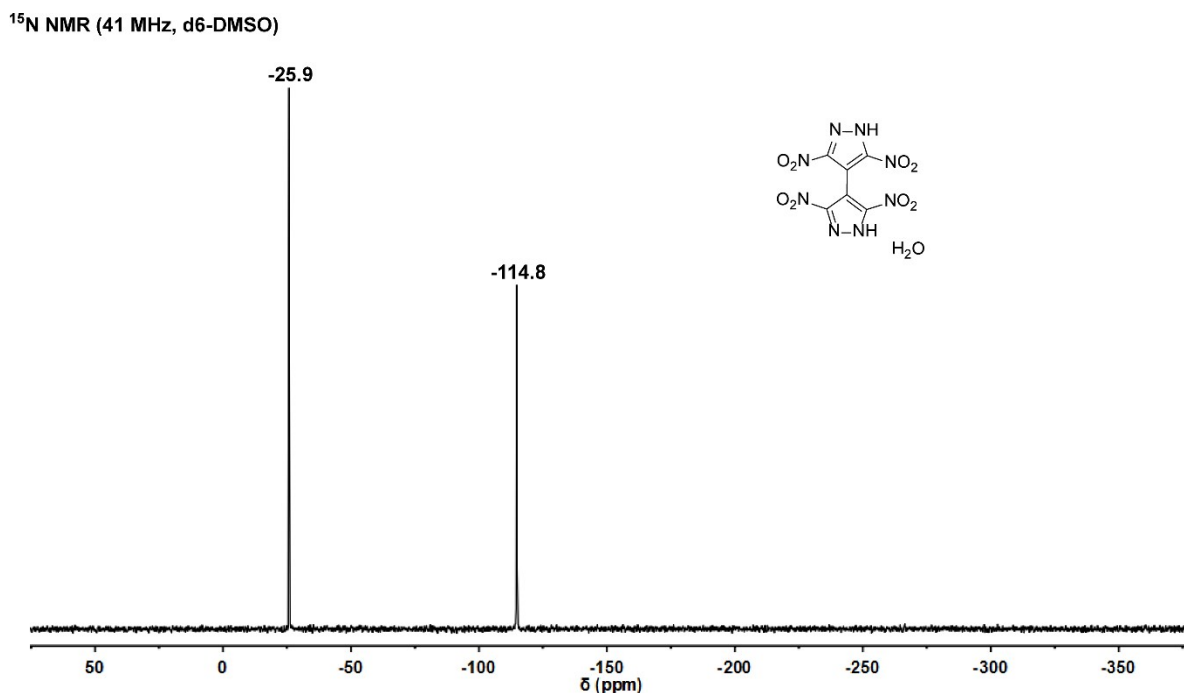


Figure S30.  $^1\text{H}$ ,  $^{15}\text{N}$  HMBC spectrum of 3,3',5-trinitro-4,4'-bipyrazole (5).



**Figure S31.** <sup>15</sup>N NMR spectrum of 3,3',5,5'-tetranitro-4,4'-bipyrazole monohydrate ( $6 \cdot \text{H}_2\text{O}$ ).

## References

- [S1] a) Reichel & Partner GmbH, <http://www.reichelt-partner.de>; b) Test methods according to the UN Recommendations on the Transport of Dangerous Goods, Manual of Test and Criteria, 4th edn., United Nations Publication, New York and Geneva, **2003**, ISBN 92–1-139087 7, Sales No. E.03.VIII.2; 13.4.2 Test 3 a (ii) BAM Fallhammer.
- [S2] I. Boldog, E.B. Rusanov, A.N. Chernega, J. Sieler, K.V. Domasevitch, *Angew. Chem. Int. Ed.* **2001**, *40*, 3435-3438.
- [S3] A.W. Johnson, *J. Chem. Soc.* **1946**, 1009-1014.
- [S4] I. Iwai, K. Tomita, *Chem. Pharm. Bull.* **1961**, *9*, 976-979.
- [S5] D. H. R. Barton, C.C. Dawes, G. Franceschi, M. Foglio, S.V. Ley, *J. Chem. Soc. Perkin Trans I* **1980**, 643.
- [S6] M.F. Fegley, N.M. Bortnick, C.H. McKeever, *J. Am. Chem. Soc.*, **1957**, *79*, 4140-4144.
- [S7] Z. Arnold, *Collect. Czech. Chem. Commun.* **1962**, *27*, 2993-2995.
- [S8] Stoe & Cie. *IPDS software*. Stoe & Cie, **2000**, Darmstadt, Germany.
- [S9] a) G. M. Sheldrick, *Acta Crystallogr.* **2008**, *A64*, 112-122. b) G. M. Sheldrick, *Acta Crystallogr.* **2015**, *C71*, 3-8.
- [S10] K. Brandenburg, *Diamond 2.1e*, Crystal Impact GbR, Bonn, **1999**.

- [S11] a) V. A. Blatov, TOPOS, *IUCr CompComm Newsletter* **2006**, 7, 4; b) V. A. Blatov, A. P. Shevchenko, V. N. Serezhkin, *J. Appl. Crystallogr.* **2000**, 33, 1193.
- [S12] I. Boldog, J.-C. Daran, A.N. Chernega, E.B. Rusanov, H. Krautscheid, K.V. Domasevitch, *Cryst. Growth Des.* **2009**, 9, 2895-2905.
- [S13] a) N. Mosca, R. Vismara, J. A. Fernandes, S. Casassa, K. V. Domasevitch, E. Bailón-García, F. J. Maldonado-Hódar, C. Pettinari, S. Galli, *Cryst. Growth Des.* **2017**, 17, 3854-3867; b) I. Boldog, J. Sieler, A.N. Chernega, K.V. Domasevitch, *Inorg. Chim. Acta*, **2002**, 338, 69-77.
- [S14] J. W. A. M. Janssen, C. C. Kruse, H. J. Koeners, C.L. Habraken, *J. Heterocycl. Chem.* **1973**, 10, 1055-1058.
- [S15] J. D. Dunitz, V. Schomaker, K. N. Trueblood, *J. Phys. Chem.*, **1988**, 92, 856.
- [S16] V. Schomaker, K. N. Trueblood, *Acta Crystallogr., Sect. B: Structural Science, Crystal Engineering and Materials*, **1998**, 54, 507.
- [S17] A. Bauzá, A.V. Sharko, G.A. Senchyk, E.B. Rusanov, A. Frontera, K.V. Domasevitch, *CrystEngComm* **2017**, 19, 1933-1937.
- [S18] M.-X. Zhang, P. E. Eaton, R. Gilardi, *Angew. Chem. Int. Ed.*, **2000**, 39, 401.
- [S19] M. J. Frisch, G. W. Trucks, B. Schlegel, G. E. Scuseria, M. A. Robb, J. R. Cheeseman, G. Scalmani, V. Barone, B. Mennucci, G. A. Petersson, H. Nakatsuji, M. Caricato, X. Li, H.P. Hratchian, A. F. Izmaylov, J. Bloino, G. Zheng, J. L. Sonnenberg, M. Hada, M. Ehara, K. Toyota, R. Fukuda, J. Hasegawa, M. Ishida, T. Nakajima, Y. Honda, O. Kitao, H. Nakai, T. Vreven, J. A. Montgomery, Jr., J. E. Peralta, F. Ogliaro, M. Bearpark, J. J. Heyd, E. Brothers, K. N. Kudin, V. N. Staroverov, R. Kobayashi, J. Normand, K. Raghavachari, A. Rendell, J. C. Burant, S. S. Iyengar, J. Tomasi, M. Cossi, N. Rega, J. M. Millam, M. Klene, J. E. Knox, J. B. Cross, V. Bakken, C. Adamo, J. Jaramillo, R. Gomperts, R. E. Stratmann, O. Yazyev, A. J. Austin, R. Cammi, C. Pomelli, J. W. Ochterski, R. L. Martin, K. Morokuma, V. G. Zakrzewski, G. A. Voth, P. Salvador, J. J. Dannenberg, S. Dapprich, A. D. Daniels, O. Farkas, J.B. Foresman, J. V. Ortiz, J. Cioslowski, D. J. Fox, Gaussian 09 A.02, Gaussian, Inc., Wallingford, CT, USA, **2009**.
- [S20] a) J. W. Ochterski, G. A. Petersson, and J. A. Montgomery Jr., *J. Chem. Phys.* **1996**, 104, 2598-2619; b) J. A. Montgomery Jr., M. J. Frisch, J. W. Ochterski G. A. Petersson, *J. Chem. Phys.* **2000**, 112, 6532-6542.
- [S21] a) L. A. Curtiss, K. Raghavachari, P. C. Redfern, J. A. Pople, *J. Chem. Phys.* **1997**, 106, 1063-1079; b) E. F. C. Byrd, B. M. Rice, *J. Phys. Chem. A* **2006**, 110, 1005-1013; c) B. M. Rice, S. V. Pai, *Comb. Flame* **1999**, 118, 445-458.
- [S22] P. J. Linstrom, W. G. Mallard, *National Institute of Standards and Technology*, Gaithersburg MD, 20899.

- [S23] a) F. Trouton, *Philos. Mag. (1876-1900)* **1884**, *18*, 54-57; b) M. S. Westwell, M. S. Searle, D. J. Wales, D. H. Williams, *J. Am. Chem. Soc.* **1995**, *117*, 5013-5015.
- [S24] M. Sućeska, *EXPLO5 Version 6.03 User's Guide*, Zagreb, Croatia: OZM; **2015**.
- [S25] a) R. Meyer, J. Köhler, A. Homburg, *Explosives*, 6th edn., Wiley, Weinheim, 2007, p. 291-292; b) T. M. Klapötke, *Chemistry of High-Energy Materials*, Walter de Gruyter, Berlin, **2015**;
- [S26] a) H. W. Sandusky, R. H. Granholm, D. G. Bohl, IHTR 2701, Naval Surface Warfare Center, Indian Head Division, MD, USA, August 12, **2005**; b) J. E. Felts, H. W. Sandusky, R. H. Granholm, *AIP Conf. Proc.* **2009**, *1195*, 233-236.
- [S27] T. M. Klapötke, T. G. Witkowski, *ChemPlusChem* **2016**, *81*, 357-360.